

General Disclaimer

One or more of the Following Statements may affect this Document

- This document has been reproduced from the best copy furnished by the organizational source. It is being released in the interest of making available as much information as possible.
- This document may contain data, which exceeds the sheet parameters. It was furnished in this condition by the organizational source and is the best copy available.
- This document may contain tone-on-tone or color graphs, charts and/or pictures, which have been reproduced in black and white.
- This document is paginated as submitted by the original source.
- Portions of this document are not fully legible due to the historical nature of some of the material. However, it is the best reproduction available from the original submission.

**NASA TECHNICAL
MEMORANDUM**

NASA TM X-73437

NASA TM X-73437

(NASA-TM-X-73437) THE USE OF ANALYTICAL
SURFACE TOOLS IN THE FUNDAMENTAL STUDY OF
WEAR (NASA) 64 p HC A04/MF A01 CSCI 201

N77-19901

**Unclas
G3/76 21607**

**THE USE OF ANALYTICAL SURFACE TOOLS IN THE
FUNDAMENTAL STUDY OF WEAR**

by Donald H. Buckley
Lewis Research Center
Cleveland, Ohio 44135

**TECHNICAL PAPER to be presented at
International Conference on Wear of Materials
sponsored by the American Society of Mechanical Engineers
St. Louis, Missouri, April 25-27, 1977**



THE USE OF ANALYTICAL SURFACE TOOLS IN THE FUNDAMENTAL STUDY OF WEAR

by Donald H. Buckley

National Aeronautics and Space Administration
Lewis Research Center
Cleveland, Ohio 44135

ABSTRACT

This paper reviews the various techniques and surface tools available for the study of the atomic nature of the wear of materials. These include chemical etching, x-ray diffraction, electron diffraction, scanning electron microscopy, low-energy electron diffraction, Auger emission spectroscopy analysis, electron spectroscopy for chemical analysis, field ion microscopy, and the atom probe. Properties of the surface and wear surface regions which effect wear such as surface energy, crystal structure, crystallographic orientation, mode of dislocation behavior, and cohesive binding are discussed. A number of mechanisms involved in the generation of wear particles are identified with the aid of the aforementioned tools.

INTRODUCTION

In 1946 Raynor Holm postulated a wear theory based upon a consideration of wear at the atomic level and atom to atom interactions across the interface between two contacting solids [1].¹ At that point in the history of the study of wear the theory could not be tested experimentally and therefore was not widely accepted as a means for predicting wear. Later, Burwell and Strong [2], Archard [3], and Krushchov and Babichev [4] set forth wear theories considering some of the same material parameters as Holm, namely load and hardness but did so on a macroscopic

¹Numbers in brackets designate References at end of paper.

rather than atomic level. These theories were widely accepted because they dealt with wear that could be readily seen with nothing more than the naked eye or for the research worker with an ordinary optical microscope.

A consideration of the atomic nature of the wear process was again introduced into wear theories by Rabinowicz [5] in the late 1950's. In this hybrid wear theory the atomic nature of the surface in the form of surface energy was considered along with a bulk mechanical property, namely, the flow pressure or resistance of the material to bulk deformation. This theory has been widely considered because of its simplicity and the ready availability of the terms needed for the equation.

Some recent wear theories, that for example, of Suh [6] and Vijn [7] have given consideration to the atomic nature of materials. The former in the form of dislocation behavior and the latter in considering atomic cohesive binding energies.

The objective of this paper is to review the fundamental nature of the wear process and those elemental properties of materials which exert an influence on the generation of wear as seen with surface analytical tools. Wear will be considered at the atomistic level with primary emphasis being placed upon experimental data with reference to theories as the data may apply thereto. The surface tools which are presently in use to study the fundamental nature of wear shall be described and results obtained with those presented.

DEFINING WEAR

The Scientific Research Committee of the OECD (Organization for Economic Cooperation and Development) has defined wear as "the progres-

sive loss of substance from the operating surface of a body occurring as a result of relative motion at the surface" [8]. The definition clearly relates wear to the surface of materials. While the definition does not account for wear in electrical contacts, it does establish that the nature of surfaces should be considered in attempting to understand wear.

SOLID SURFACES

While those solids which undergo wear can consist of a wide variety of materials both crystalline and noncrystalline wear is most frequently encountered with crystalline solids. With elemental metals the surface will consist of the interface between the outer most layer of atoms which is not bound by a layer of like atoms and the foreign medium to which that layer is exposed. For alloys the surface may be more complex containing a number of different elements or a particular element, which because of energy considerations chooses to segregate at the surface.

The atoms in the surface layer of a metal may be thought of as spheres. An examination of the crystal structure of metals indicates that the packing arrangement of the spheres can vary and will depending upon the exposed orientation to the surface. Fig. 1 presents two possible packing arrangements of atoms in surface layers.

In Fig. 1(a) the atoms in the surface layer are arranged in such a fashion that each atom is in contact in the surface layer with four like atoms forming a square packing array as indicated by R and the sketch. In the face centered cubic crystal structure seen for such metals as copper and nickel this represents a crystallographically noted (100) surface. Atomic packing details for the surfaces of crystalline mate-

rials can be found in reference [9] and for crystallographic notations in reference [10].

Another form of atom packing in surface layers is characterized as the hexagonal close packed array presented in Fig. 1(b). Each atom is contacted by six of its neighbors in the surface layer as indicated by R and the hexagon. This form of packing is the most efficient and is the form used by squirrels in storing their nuts and bees in making hives. It is also the packing array seen for (111) crystallographic planes in face centered cubic metals and the (0001) planes in hexagonal close packed metals.

The hexagonal close packed array of surface atoms seen in Fig. 1(b) is the planes in face centered cubic, body centered cubic and close packed hexagonal metals exhibiting the strongest interplanar bonding strengths and the weakest bonding strengths between adjacent like planes. For this reason deformation of metals occurs via slip between these planes. They also exhibit the lowest surface energies as shall be discussed later and lower adhesion bonding forces and friction than other crystallographic orientations.

The arrangement of atoms in metal crystals as seen in Fig. 1 applies to packing as seen in a perfect surface. Real metal surfaces are not perfect but contain many defects. Some of these defects are sufficiently large, such as dislocations, so as to be observable with ordinary electron microscopy while others are of such a size as to require the field ion microscope for their observation.

Some of the defects observed on metal surfaces are indicated in

Fig. 2. When an atom is missing from a lattice site of the surface a hole or vacancy is created. Vacancies can exist not only in the surface but in the bulk metal as well. The presence of an atom on the surface due to adsorption of foreign atoms onto the surface or segregation to the surface from the bulk will result in the presence of adatoms. These two defects are idealistically pictured in Fig. 2. Their presence creates localized disturbances in surface lattice energetics.

Vacancies can condense into line defects along rows of atoms in the bulk. These defects known as dislocations can emerge at the surface. They can be one of two types, either edge or screw dislocation; their name coming from the manner of their formation. When such defects egress from the bulk to the surface they generate a defect in the surface as indicated for a screw dislocation in Fig. 2.

When metals or alloys are cooled from their melts to solidification the presence of localized sites which interfere with normal crystal growth frequently called nucleation sites result in lattice atom packing disregistry. This disregistry will permeate the entire solid with the formation of a variety of atom packing (crystallographic) orientations adjacent to each other in the bulk and at the surface. These then, make up the individual grains of the solid. On the surface each grain has a different lattice packing or crystallographic orientation (Fig. 1) from its nearest neighbors.

The array of grain orientations at the surface are connected by boundaries (Fig. 2) which serve to accommodate the mismatch in grain orientations. The greater the mismatch the narrower will be the number

of rows of atoms required to accommodate the mismatch. At the surface because of the strain in the grain boundary lattice resulting from accommodation of the two grain orientations on either side of the boundary, a highly energetic state exists which differs from that of the adjacent grains.

Most real surfaces are not flat and smooth but contain surface irregularities or asperities [12]. Bearing in mind that surfaces contain these gross irregularities there are below these, defects smaller in size, and these include fracture steps either ductile or brittle and cleavage steps as indicated in Fig. 2.

INTERFACES

When two solids, for example metals, are brought into contact an interface is established from the surface of the two solids and this interface plays an important role in wear.

With two metallic surfaces brought into close proximity and contact, both long range interactions as a result of Van der Waals and electrostatic forces and short range interactions arising from chemical bonding of the two surfaces exist. These forces constitute the interfacial binding energy of the metals to each other when brought into solid state contact. The amount of work necessary to overcome the interfacial bonds is then the force or energy of adhesion that develops at the interface between the two solid surfaces.

The jellium model has been used to consider charge densities of the metal surface in vacuum for close-packed planes. This model has been recently applied to adhesion at a bimetallic interface [14]. If two dissimilar metals are considered (e.g., aluminum and zinc) the electron

density overlaps in the interface can be represented as indicated in Fig. 3.

In Fig. 3, n_1 and n_2 represent the vacuum-metal electron density numbers for zinc and aluminum, y is the direction normal to the interface, a_0 is the separation between the surfaces, and $n_+^{(1)}$ and $n_+^{(2)}$ are the jellium positive charge densities for zinc and aluminum.

In considering adhesion at a bimetallic interface, all the energy sources for bonding must be taken into account. This is done for the Al-Zn couple in Fig. 4. The energy for the various bonding sources is presented as a function of separation in atomic units. The equilibrium or minimum energy position is indicated by a_0 .

Coupling the concept of the jellium approach to bonding with a consideration for lattice mismatch, the authors of reference [14] calculated the binding energy for a number of bimetallic couples. The theoretically calculated values agreed well with experimental results.

Comparison of the calculated energies of adhesion or bimetallic binding energies with surface energies indicate that there is an overlap. Thus, the Al-Zn binding energy is lower than the Zn-Zn surface energy but larger than the Al-Al surface energy. One might therefore predict that lower-surface-energy metals will transfer to higher-surface-energy metals on solid state contact with subsequent separation of the surfaces.

When two atomically clean metals are placed into contact, adhesion has been always observed to occur. Further, on separation of the surfaces the cohesively weaker metal has generally been observed to transfer to the cohesively stronger [15]. In general, cohesive energies and

surface energies correlate.

Bonding at the interface, adhesion and transfer across the interface are extremely important in understanding wear. Frequently these processes occur at the atomic level and it is therefore necessary to examine surfaces in contact at this level.

SURFACE TOOLS

Field Ion Microscopy

The field ion microscope (FIM) is a research tool of relatively recent origin having been invented by Mueller in 1951 [13]. The microscope is truly unique in that it is the only device available today which will allow the examination of individual atom sites and surface structures in atomic detail. It has an atomic resolution of 2.5 \AA .

The field ion microscope in and of itself is relatively simple in construction and concept. Incorporated into an adhesion experiment to study the adhesion of one solid to another, it can lend considerable insight into adhesion the forerunner of adhesive wear. Fig. 5 is a schematic diagram of the field ion microscope used in adhesion studies [16].

In the field ion microscope a wire hemispherically tipped with a 250 to 500 \AA radius is generated by electro-etching one end of the wire. This tip is the pin shaped specimen indicated in Fig. 5. The vacuum system of Fig. 5 is evacuated and then back filled with helium to a pressure of 10^{-3} torr. The surface is cleaned by applying a high positive electric field at the tip of sufficient strength to tear atoms away from the surface (field evaporation). This cleaning process creates a near perfect hemispherical surface by removing asperities and other im-

perfections from the surface. The tip is then biased to a high positive potential relative to a phosphor-coated fiber optic window located 10 cm away. This produces a magnification of the tip of from 1 to 3 million.

Fig. 6 demonstrates the basic principle of operation of the FIM. A helium atom impinging on the tip experiences a very high electric field resulting from the curvature of the tip. This field polarizes the atom and distorts the atomic potential enough so that there is a reasonable probability that an electron will tunnel from the atom to the metal leaving behind a helium ion. The atom hops on the surface several times until it is accommodated at a distance sufficient for the tunneling to occur. If it gets too close (dashed line) the atomic energy level lies below the Fermi Energy leaving no states to tunnel to. This ionization occurs directly above atoms located in the tip where the field is highest. For the most part only 10 to 15 percent of the atoms on the tip located at the zone edges and at the kink sites are visible. These ions are then accelerated to the phosphorescent screen at a distance of 10 cm from the tip giving the high magnification. The FIM gives much higher resolution than the field electron microscope (2.5 \AA as compared to 25 \AA), since the lateral uncertainty in position is much lower with ions and the thermal part of this uncertainty in position can be lowered by cooling the tip to liquid hydrogen or liquid helium temperatures.

Fig. 7 is a typical FIM pattern for a clean tungsten tip oriented in the (110) direction. The small rings are various crystallographic planes that would appear on the hemispherical surface. Each white spot is an individual atom site. Vacancies and interstitials on the surface can be detected in the FIM.

Adhesion experiments were conducted in the FIM by compressing a bellows in the tubulation on the left side in Fig. 5. The bellows compression moves a beam containing a flat specimen under the pin specimen. The flat is brought into contact with the pin tip by deflection of the beam with electromagnets. Both load and adhesive bonding forces are measured with the current drawn by the electromagnets. A microbalance with a sensitivity to loads as low as 0.05 milligram has been used in place of the electromagnets. A photocell sensing system is used to determine beam position and serves to damp out vibrations.

Atom Probe

The FIM-adhesion apparatus of Fig. 5 has incorporated into it one atom probe. The atom probe provides the ultimate in chemical analysis of a surface in that it furnishes a way of identifying a single atom.

A long tube is mounted to the specimen region of Fig. 5. A very small hole is placed in a plate a short distance away from the pin specimen. The surface is imaged and the particular atom on the surface whose chemistry is desired is positioned over the hole. The surface is then field evaporated. In the vacuum the atoms leave the surface and travel in straight paths with the particular atom of interest passing through the hole and down the tube to a time of flight mass spectrometer where the elemental identity of the atom is determined. Thus, the FIM used with an atom probe attached to it provides both structural and chemical analysis at the atomic level.

LEED (Low Energy Electron Diffraction)

Electron diffraction was experimentally demonstrated by Davison and Germer in 1927 [17]. Davison and Germer showed that as a result of the

wave nature of an electron, the electrons could be diffracted by a crystal lattice in a manner similar to x-ray diffraction. Following this early work only H. E. Farnsworth at Brown University pursued the technique as a surface analytical tool using a Faraday cup to detect the diffracted electrons [18]. The reason that low energy electrons (0 to 200 eV) can be used to examine surfaces is that the penetration of these electrons should be limited to the first few atomic layers. LEED became a popular surface analytic tool in the late 1950's when L. H. Germer of the Davison-Germer experiment suggested that the diffraction pattern could be displayed on a fluorescent screen by post-accelerating the diffracted electrons.

Fig. 8 indicates simply the diffraction process in LEED if the crystal were a two-dimensional lattice. An electron gun shoots a beam of electrons of a given energy at the crystal. The electrons are diffracted by the lattice and the diffraction pattern is observed on the fluorescent screen.

An example of a LEED pattern, Fig. 9 shows the LEED pattern of a clean (110) tungsten surface. The diffraction pattern has the characteristic symmetry of a bcc (110) surface in the direct lattice. The LEED pattern on the right is the pattern which results when what is thought to be 1/2 monolayer of oxygen is adsorbed on the surface. Note the additional spots located at (1/2, 1/2) positions. In the direct lattice these represent rows of atoms with double the spacing of the substrate. Additional comments are necessary regarding the interpretation of LEED patterns. Since the pattern is in the reciprocal lattice you cannot unambiguously arrive at a direct lattice structure without examining spot in-

tensities as in x-ray diffraction. The interpretation of LEED patterns is presently a subject of intense study. In some cases simple interpretations seem to be valid, in others they are not. For an excellent review of LEED the reader is referred to reference [19].

Auger Emission Spectroscopy

Auger electron spectroscopy (AES) was suggested as a tool for performing surface chemical analysis in 1953 by Lander [20]. However, it did not become a popular surface analytical tool until the late 1960's when L. A. Harris suggested that electronic techniques for extracting small signals from a large background be applied to Auger analysis [21].

The first step in the Auger process is excitation of the atom to be detected. Then the radiation must be energy analyzed. The resulting spectrum must be detected and then analyzed for the species present. In Fig. 10 the basic Auger process is described. First an inner level is ionized. An electron drops from an upper level and releases a fixed quantity of energy equal to the difference in energy of the two levels. This energy is absorbed by an electron in an upper level and if the energy of this electron is sufficient, it can escape from the solid. In general the higher the atomic number of the material, the more peaks available for analysis. However, the higher the atomic number, the lower the probability that an Auger electron will be emitted from the material as opposed to an x-ray. All elements except hydrogen and helium can be detected with AES. AES is a surface sensitive tool since the energies of the electrons studied are sufficiently low that they can only originate from a few atomic layers. The sensitivity of AES is of the order of 0.01 monolayers.

Fig. 11 is a sample spectrum obtained with an Auger emission spectrometer. The spectrum is for an iron (001) surface with adsorbed ethylene and peaks for both iron and carbon from the ethylene are detected. The technique developed by Harris for filtering out the Auger electron energies by the use of the derivative of electron energy distribution is used.

There are two types of Auger emission spectroscopy apparatus in general use. For a detailed discussion of these the reader is referred to reference [22].

In one of the systems which is frequently used in conjunction with LEED the screen for the LEED (see Fig. 8) is used for the detection of Auger electrons. Such a combined LEED-Auger system has been incorporated in an adhesion apparatus for the study of the atomic nature of the transfer of material from one surface to another as a result of adhesion (adhesive wear). The system is shown schematically in Fig. 12.

There are two electron guns in Fig. 12, one for the generation of the low energy electrons associated with LEED and a second higher energy side gun for the production of Auger electrons. An ion gun is also in the system for argon ion bombardment of surfaces to achieve atomic cleanliness. Much like with the FIM a beam contains a second specimen for adhesion studies. LEED patterns (Fig. 9) are photographed through a window and Auger traces (Fig. 11) are obtained on the graph paper of an x-y recorder.

The second type of Auger spectroscopy system is the cylindrical mirror analyzer shown in Fig. 13. With this analyzer the electron gun for the generation of Auger electrons is incorporated directly into the

analyzer. The CMA has a higher signal to noise ratio and sensitivity than the LEED, Auger analyzer. The improved signal to noise ratio reduces the need for output filtering and thus allows for very fast sweep (0.1 sec) and thus the entire elemental spectrum can be displayed on an oscilloscope.

The fast response time of 0.1 second to display the elements present on a surface make the CMA ideally suited for the study of wear dynamically. Such a spectrometer has been incorporated into friction and wear devices as indicated in Fig. 14. The specimens in Fig. 14 are of the pin on disk configuration.

The CMA of Fig. 14 has its analyzing beam positioned approximately 150 degrees away from the position of pin and disk contact. The beam of the CMA can be deflected so as to allow for analysis inside and outside the wear track during sliding. Such a capability provides a detailed chemical insight into the wear process. Further, lubricating species can be admitted into the system and their interaction with the surface readily detected. The CMA is a surface tool analyzing only the outermost atomic layers.

ESCA (Electron Spectroscopy for Chemical Analysis)

Another surface tool available for the study of wear is ESCA (Electron Spectroscopy for Chemical Analysis). This technique for surface analysis was originated by Siegbahn and coworkers in Sweden [23]. For a good capsule review of ESCA and its capabilities the reader is referred to reference [24].

ESCA like LEED and AES requires the use of a vacuum environment. In

ESCA a wear surface on wear debris is exposed to a beam of monochromatic x-rays causing electrons with kinetic energies of the parent atom to be ejected from the specimen. A spectrum containing the characteristic probes for the elements present is obtained by plotting the total number of electrons ejected from the surface as a function of kinetic energy. ESCA will analyze the surface to a depth of about 20 Å and has sufficient sensitivity to permit the detection of fractions of a monolayer.

An ESCA system which has been used to analyze wear surfaces in extreme pressure additive studies is indicated schematically in Fig. 15 and was obtained from reference [25]. A beam of x-rays from the tube strikes the sample specimen and the photoelectrons are emitted from the surface. They pass through both spherical and cylindrical condensers to an electron multiplier. Both a counter and minicomputer are employed in the detection system. The electrons as a function of their energy are then plotted on X-Y recorder.

There are a number of variations of the ESCA system presented in Fig. 15. Some devices employ both ESCA and AES in the same system. AES provides a good technique for elemental analysis while ESCA provides chemical binding information.

Thus, with ESCA it is possible from binding energies to identify the nature of the compounds in which the elements exist on the surface. The binding energy of the ejected electrons from the surface is determined by their chemical environment and is roughly a function of the atomic charge.

In one ESCA system, which contains AES an ion gun is used to

sputter etch away surface layers and thereby permit doing a depth profile analysis of surface films. The outermost layers of wear surfaces after sliding or rubbing in an oil-additive environment consists of the adsorbed oil and frequently carbon is the principal peaks detected. It is usually only after sputter etching away this layer that the compounds formed by additive interaction with the metal are detected.

Fig. 16 is an ESCA spectrum for iron surface exposed to one percent dibenyl disulfide in mineral oil at 250° C for one minute. From the spectrum the presence of oxygen, carbon, sulfur, and iron are seen.

Considerable work has been done to correlate the chemical shifts of ESCA with the molecular structure of organic compounds, particularly of those structures containing carbon, nitrogen, sulfur, and phosphorus [26]. Such information can be very useful in the determination of lubricating structures on wear surfaces.

The chemical shifts or shifts in binding energy for the carbon 1s electron can, for example, be identified with the functional group from which the carbon came as indicated in Fig. 17. From Fig. 17 carbon to nitrogen, oxygen bromine, fluorine, and sulfur bonding can readily be distinguished by shifts in binding energies from carbon to carbon bonding. Further, whether oxygen is singly or doubly bonded to oxygen is readily discernible in the figure.

SEM (Scanning Electron Microscopy)

Probably the single most useful surface tool available to the tri-biologist interested in the study of wear is the SEM (Scanning Electron Microscope). This is so because it requires the least amount of technical

expertise for the interpretation of the results and it presents a physical picture of the wear surface.

The principle of the SEM is indicated in the block diagram of Fig. 18. Electrons from an emission source or filament are accelerated by a voltage commonly in the range of 1 to 30 kV and directed down the center of an electron optical column consisting of two or three magnetic lenses. These lenses cause a fine electron beam to be focused onto the specimen surface. Scanning coils placed before the final lens cause the electron spot to be scanned across the specimen surface in the form of a square raster, similar to that on a television screen. The currents passing through the scanning coils are made to pass through the corresponding deflection coils of a cathode ray tube - so as to produce a similar but larger raster on the viewing screen in a synchronous fashion [27].

The electron beam incident on the specimen surface causes various phenomena, of which the emission of secondary electrons is used. The emitted electrons strike the collector and the resulting current is amplified and used to modulate the brightness of the cathode ray tube. The times associated with the emission and collection of the secondary electrons are negligibly small compared with the times associated with the scanning of the incident electron beam across the specimen surface. Hence, there is a one-to-one correspondence between the number of secondary electrons collected from any particular point on the specimen surface and the brightness of the analogous point on the screen. Consequently, an image of the surface is progressively built up on the screen.

The SEM has no imaging lenses in the true sense of the word. The

image magnification is determined solely by the ratio of the sizes of the rasters on the screen and on the specimen surface. In order to increase the magnification, it is only necessary to reduce the currents in the SEM scanning coils. For example, if the image on the CRT screen is 10 cm across, magnifications of 100 \times , 1000 \times , and 10 000 \times are obtained by scanning the specimen 1 mm, 0.1 mm, and 0.01 mm across, respectively. One consequence of this is that high magnifications are easy to obtain with the SEM, while very low magnifications are difficult. Thus, for a magnification of 10 \times it would be necessary to scan a specimen approximately 10 mm across, and this presents difficulties because of the large deflection angles required. For instance, the electron beam may strike the lens pole pieces or aperture, and at the extremes of the scan, linearity may not be maintained.

The completely different operation of the SEM compared to most other microscopes is possible because there are no imaging lenses, and any signal that arises from the action of the incident electron beam (reflected electron, transmitted electrons, emitted light, etc.) can be used to form an image on the screen.

An apparatus for the study of friction and wear has been incorporated directly into the SEM to allow observation of the wear process which it is developing. Fig. 19 is a schematic of the apparatus. A disk specimen 1.9 cm in diameter is mounted on an adapter to the rotary specimen feed-through. The surface of the disk is inclined at approximately 70 degrees with respect to the electron beam. This steep angle permits the interface to be viewed from a near side view. A variable speed electric motor

and gear train is attached to the external rotary specimen feedthrough to provide rotation of the disk from 0.001 to 5 rpm. The rotation can either be clockwise or counterclockwise to provide for SEM observation of either the prow or wake of the rider disk contact and a direct observation of the wear process while it is occurring. In addition, a side view of the wearing process can be observed.

The stylus is mounted in an arm which can be moved in and out as well as up and down and laterally by means of a bellows and gimbal system. The gimbal system is comprised of a precision optical orientor which is mounted on a translational stage. This stage and the optical orientor are micrometer controlled thereby allowing very precise positioning of the rider on the disk under the scanning beam.

The arm in which the stylus is mounted contains two flex bands of beryllium-copper upon which strain gages are attached. The normal loading is accomplished by allowing the magnets which are mounted on the optical orientor ring to pull the arm downward to the disk surface.

The strain gage output of the load sensing gage is amplified and displayed on a digital millivolt meter which with suitable calibration provides for a direct reading of the load being applied. The friction force gage is read out either on a strip chart recorder or oscilloscope to provide for the observation of the friction trace which is more transient in nature.

The entire wear experiment is viewed on the television monitor of the SEM and the video signal is recorded along with audio comments on video tape to provide for data recording. The tape can be played back in

slow motion and stop action to facilitate interpretation. In addition kinescopic motion pictures can readily be made from the video tape.

To provide for an analysis of the wear track, an energy dispersive x-ray analyzer is mounted on the SEM. The analyzer has 400 channels and a resolution of 170 electron volts. Also provided is the capability of elemental mapping.

Fig. 20 is a photograph of the wear track generated on a tungsten carbide surface by a diamond stylus. The photomicrograph was obtained during the sliding process. The fracture cracks seen in the photomicrograph were observed during their formation as was the generation of wear particles.

The use of energy dispersive x-ray analysis in conjunction with the SEM permits the direct analysis elementally of the wear surface and wear debris. For example, the wear debris generated in experiments with tungsten carbide cermets containing various percentages of cobalt binder were examined with the x-ray technique. Fig. 21 is x-ray profiles of the wear debris from two of the cermet compositions.

In Fig. 21 the peaks at 8.39 KeV are due to the tungsten $L\alpha$ line and those at 6.92 KeV are for cobalt. The white dots are the intensities for the elements in the wear debris while the white bar represents the unworn surface. For both compositions there was a 22 percent higher concentration of cobalt in wear track and debris than was found on the unworn surface indicating that the binder had smeared out over the wear surface. It was substantiated as smearing by the use of etching techniques [28].

Other Surface Tools

In addition to those surface tools already described and used in wear studies there are others also available. Some of these use phonons, others electrons and still others ions as sources of excitation for analysis. Likewise the detection systems may be based upon the analysis of electrons, phonons, or ions.

A summary of surface tools currently available, their excitation and detection modes is presented in Fig. 22. Many of these techniques are described in more detail in reference [29] from where Fig. 22 was obtained.

SURFACE ENERGY

Concept

If the surfaces of solids are important in wear, then the energetics of surfaces must be considered. One wear theory, namely that of Rabinowicz required the incorporation of surface energy in the determination of wear particle size [5].

What is surface energy? It is simply the work required to pull apart a solid at 0° K and thereby generate a new surface. More specifically for a crystalline solid it is the energy to cleave a crystal parallel to a crystal plane and form a unit area of new surface. A classical example for the determination of surface energy is to consider the crystalline solid diamond. The cleavage energy per square centimeter may be simply considered as the number of bonds that must be broken over that area. Thus, for the (111) plane of diamond there are 1.73×10^{15} bonds per square centimeter and with a bond energy of 90 kcal one obtains a sur-

face energy of 5400 ergs per square centimeter. With the (100) plane of that same solid the value becomes 9140 ergs per square centimeter because of the higher density of surface atoms [31].

Since the atomic packing in various planes of crystalline solids differs it might be anticipated that, at least from a theoretical point of view, the surface energy for these various planes would vary. Gilman has calculated the surface energy for a number of crystalline solids and for various planes of those solids [32]. Some representative values are presented in Table I. From the data it is apparent that surface energy, like hardness and modulus of elasticity is anisotropic.

Most engineering materials are polycrystalline and therefore a variety of orientations can and do exist on the surface with corresponding differences in surface energy and grain boundary energies. Rolling, drawing, compressing, machining, and forging can all result in preferred orientation of grains on a surface commonly called texturing [33]. It can also occur as a result of sliding [34]. In considering or selecting surface energy values these factors must be taken in account. For a review of the subject of the influence of crystallographic anisotropy on surface energy, the reader is referred to reference [34]. The subject has also been examined very recently [36].

Methods of Measurement

Surface energies for solids have been measured by various techniques for over thirty years. It is, however, safe to say that reliable measured values for the surface energy of metals do not exist. The principle reason for this is the lack of adequate control of impurities in metals.

In Fig. 23 the effect of sulfur on the surface energy (tension) of iron in the liquid state is presented. The surface energy (tension) decreases drastically with sulfur content [37]. The effect of sulfur on the surface energy of solid iron as well as for other impurities cannot be found in the literature but it would seem reasonable to assume that sulfur would exert a similar effect on the surface of solid iron. Sulfur has been observed with Auger spectroscopy to segregate to the surface of solid iron [38].

A variety of experimental techniques have been used to experimentally determine surface energies [39]. These include (1) twin boundary thermal grooving [40], (2) wedge floating [41], (3) smoothing of surface scratches [42], (4) equilibrium shape of particles [43], (5) gas bubble formation [44], (6) pulse field emission [45], (7) field ion microscopy [46], (8) heats of solution [47], (9) ultrasonics [48], (10) zero-creep [49], and (11) cleavage [50]. Of all of these techniques the zero-creep and cleavage techniques are generally considered to be most reliable.

The zero creep technique is based upon the simple principle that a metal with a large surface to volume ratio such as a foil will shrink upon heating to high temperatures. This shrinkage is due to surface energy. The surface energy is measured by applying sufficient load to just restrain the forces of shrinkage.

While foils were originally used for the determination of surface energy, the substitution of wire for foil has increased the use of this technique [39]. It, however, suffers from the limitation that it does not provide information on the anisotropic nature of surface energy, an

important factor which cannot be overlooked.

Cleavage is the technique which supplies the surface energies for the various atomic planes of crystalline solids. Obreimoff very elegantly used this technique in 1930 to study the surface energy of mica [50]. The technique has also been very effectively used by Gilman in the study of a variety of materials, metals, and nonmetals alike [51].

Gilman with the cleavage of metal crystals, has as already discussed, indicated the anisotropic nature of surface energy. Using his technique it is possible to generate atomically smooth metal surfaces. The cleavage method has been used to generate such surfaces of zinc for friction and wear studies [52].

The importance of impurities on surface energy discussed with reference to iron earlier can be seen with the cleavage of metals and alloys. Gilman cleaved zinc single crystals and zinc crystals alloyed with one percent cadmium. This was done at various temperatures for the pure and alloyed metal with surface energies measured. The results of those measurements are presented in Fig. 24.

In Fig. 24 cleavage surface energy is plotted as a function of temperature for the zinc and zinc-cadmium alloy cleaved along the (0001) basal plane. Two observations can be made from the data. The first is that the alloy exhibited a higher surface energy than elemental zinc and secondly, the surface energy increases with increasing temperature. The first observation indicates the effect of impurities on surface energy while the second indicates the effect of the ductile to brittle transition of zinc on surface energy.

ATOMIC SURFACES AND WEAR

The fundamental atomic nature of the wear process has been studied for many years and in the early days some very elegant experimental work was accomplished with rather unsophisticated tools. Some of these early studies made use of such tools as x-ray and conventional electron diffraction. While they did not examine individual atoms, as the field ion microscope now does for us, they did provide the ability to determine atomic structural effects on wear.

Gwathmey, et al. [53] in 1948 demonstrated that the (111) planes of copper in the presence of a lead film exhibited markedly less wear than the (110) planes. The abrasive wear behavior of both copper and iron had been studied early with regard to the influences of translational and rotational slip of the atomic slip planes [54]. In the polishing of even a hard material like diamond, Seal and Menter found that wear groove formation was sensitive to crystallographic direction and that because of observed crystallographic slip diamond undergoes plastic deformation in the polishing (wear) process [55].

The very fine wear experiments of Agarwala and Wilman demonstrated with ordinary electron diffraction that abrasion of iron crystal surfaces resulted in the transformation of body centered cubic α iron to face centered cubic γ iron indicating that during abrasive wear of iron the surface temperature, at least locally, reached 900° C [56,57]. Later crystal transformation was shown to effect adhesive wear for cobalt with the hexagonal form exhibiting one hundredth the wear observed for cubic cobalt [58].

The atomic nature of wear has been examined for brittle as well as for ductile materials such as the metals already discussed. The anisotropic nature of wear for magnesium oxide [59] and aluminum oxide [60] has been shown. In reference [59] a wear track was found to be deeper in the soft [100] direction than in the [110] direction on a (001) face of a magnesium oxide crystal. Kiesz demonstrated the anisotropic nature for the wear of a variety of inorganic crystals [61] and Duwell for a number of planes of rutile (TiO_2) [62].

The variation in wear rate with crystallographic orientation of rutile as measured by Duwell is presented in Fig. 25. From Fig. 25 it is evident that the wear rate of rutile can vary by a factor of seven with variations in crystallographic orientation.

The foregoing insight into the influence of the atomic crystallographic nature of materials on wear has been obtained with standard x-ray or electron diffraction techniques. Still other relatively unsophisticated tools are available for surface analysis in the study of wear.

Many properties of crystalline materials can effect wear at the atomic level, beyond atomic packing. These include the presence of interstitial or substitutional atoms which strain the crystal lattice, ordering or the lack thereof, cohesive and adhesive binding energies and defects both vacancies and dislocations. Remembering that dislocations are defects in the rows of atoms in crystalline solids and that all crystalline solids contain such defects their consideration becomes important in the understanding of wear.

The concentration of dislocations present in a crystal solid will vary with the state of the crystal. With a metal whisker only a single

screw dislocation may be present but most metal crystals will typically contain approximately 10^6 per centimeter and the number will increase with deformation of the crystal. Very low stresses are required to move dislocations through a crystal lattice. When these reach the crystal surface a slip offset one atom spacing wide develops at the surface. Should a large number of dislocations emerge at the surface having originated from the same crystal plane the slip offset will become a step which may be seen in the microscope or even with the naked eye.

Bearing in mind that the deformation process associated with crystalline materials in sliding or rubbing contact can generate these dislocation steps (commonly called slip lines or slip bands on the surface), some important implications relative to wear arise. Many investigators have experimentally observed these steps including the present author but not quite so superbly as Barquins et al. [63-65]. Such a step is shown schematically in Figs. 2 and 26(a).

The origin of these dislocation steps at the surface with deformation expose nascent, atomically clean material which can interact with the environment at the surface or a mating solid surface. Should the latter occur the initial step in the formation of an adhesive wear particle has occurred. These steps are also micro-irregularities smaller in size than asperities. With tangential motion they can be sheared resulting in the formation of wear particles.

Dislocation interactions with other dislocations or obstacles at or near the surface can also effect wear. They can in moving along a slip plane intersect, instead of with a free surface, some barrier such as an

inclusion, twin on grain boundary. When this occurs, the dislocations will coalesce and can form voids such as those observed by Steijn in the wear of ionic crystals [66]. More recently the same phenomenon has been observed with metals [6]. The pile up of dislocations at some barrier is indicated in Fig. 26(b).

In addition to the generation of subsurface voids dislocations can interact at the surface where slip planes intersect to form cracks. This is diagrammatically demonstrated in Fig. 26(c). A and B of the figure represent slip planes intersecting at point C. A crack forms at the surface where the dislocations pile up. This mechanism has been observed to operate in wear [67].

Both the subsurface developed voids or cracks and the surface originated cracks play an important role in the generation of wear as the reader probably already surmised. The subsurface cracks and/or voids can coalesce to the point where applied loads can initiate fracture from the void to the surface with the formation of a wear particle or cracks can propagate to the surface. The surface originated cracks can progress into the solid until they intersect with other surface originated cracks or subsurface voids to form wear particles.

Dislocation activity can be followed on a surface of a crystalline solid with some rather simple unsophisticated techniques. One such technique is chemical etch pitting [68]. Just as the grain boundaries at the surface are high energy sites so too on a smaller scale are the emergent sites of the dislocations. A chemical reagent will preferentially attack these sites leaving pits. The presence of dislocations can then be iden-

tified. The shape of the pit is shown schematically in Fig. 26(d). By careful examination of the pit shape insight into the atomic plane from which it came can be obtained.

The generation of new dislocations in the wear process and the movement of dislocations can be carefully followed by etch pitting. This is indicated in Fig. 26(e). The original dislocation on re-etching will be larger in size than new dislocations or those that have moved. Etch pitting has been utilized effectively in the study of wear [66, 69, 70].

The reflexion electron microscope, a forerunner of the SEM described earlier, was very effectively used by Chapman and Menter [71] in the study of micro-wear of textile fibers. These studies demonstrated the importance in having a depth of focus in the examination of wear.

In 1971 the Cambridge School conducted some very interesting experiments in the scanning electron microscope (SEM) establishing that dynamic friction and wear studies could be conducted in the SEM and that much could be learned from such experiments [72]. Such experiments later demonstrated that in all deformation of gold surfaces the crystal lattice between dislocations approached the theoretical strength of the crystalline solid [73].

The SEM has been instrumental in identifying a basic wear mechanism. In reference [74] friction and wear experiments were conducted with a polycrystalline copper slider making a single pass over a copper bicrystal surface. The wear track on the grains of the copper bicrystal, both the (111) and (210) surface orientations, revealed in the wear track the presence of cleavage or fracture cracks in the surface as indicated in

the SEM photomicrographs of Fig. 27. The leading edge of the crack has ahead of it a curl of metal which extends above the plane of the surface. These cracks and curls are present in both grains being much larger in size on the (210) surface.

Close examination of the cracks in the SEM photomicrographs of Fig. 27 indicate that the back faces of the cracks are atomically smooth. Sectioning the track and crack indicate that the angle between the crack and the surface places the existence of the cracks along (111) slip planes. These cracks form, with sliding, at room temperature.

The formation of the crack and curl of material occur via an adhesion mechanism. When the polycrystalline copper slider is placed into contact with the bicrystal surface under load adhesion occurs at the interface. With tangential motion, the slider-bicrystal interfacial bond being stronger than the cohesive bonds along (111) planes, cohesive fracture occurs along (111) slip planes. As tangential motion progresses the bicrystal surface is pulled up with the slider. At some point the crack has progressed sufficiently deep that the curl of material attached to the slider is large enough to resist further cohesive fracture and the interfacial adhesive bonds break allowing the slider to move on.

The foregoing sequence of events leaves a curl of metal projecting above the surface which is sheared off on subsequent passes of the slider generating wear particles. The entire process of adhesive wear is the result of cohesive fracture along atomic slip planes in the copper. The wear is anisotropic as indicated in the size of the cracks and curls on the two atomic planes of differing orientation and the size of the sub-

quent wear particle formed. These wear observations relate back to the discussion on surface energy anisotropy in wear. The higher atomic density lower surface energy (111) plane exhibits the lesser wear.

The anisotropic wear just described occurs not only for metals in contact with themselves such as the copper but also for dissimilar materials. Studies with PTFE (polytetrafluoroethylene) sliding against (111), (100), and (110) surface oriented single crystals of aluminum indicate anisotropic wear behavior.

When PTFE contacts the aluminum under load interfacial plastic deformation of the aluminum occurs with the fracture of the brittle aluminum oxide and contact of the PTFE with nascent aluminum. Sliding results in shear in the aluminum, which with further sliding becomes embedded in the PTFE. The embedded aluminum strain hardens and then acts as a cutting tool to score or wear the parent surface from which the particles came. Fig. 28 contains SEM photomicrographs of the embedded aluminum wear fragments.

Of the three orientations of aluminum examined the (111) plane exhibited the least wear with the (110) plane suffering the greatest wear and surface damage and the (100) orientation falling between the other two orientations in severity of surface wear. The surface energies for these planes are in the $(110) > (100) > (111)$ order and the surface hardness values in the inverse $(111) > (100) > (110)$ order.

With dissimilar metals in contact even the least active of metals such as the noble metals experience adhesive wear. This can occur at the atomic level with simple touch contact. Numerous adhesion studies by the

present author with gold contacting various other metals using LEED and AES surface analysis indicate interfacial transport from one surface to another with the cohesively weaker transferring to the cohesively stronger. The adhesive interfacial bonds appear to nearly always be stronger than the cohesive bonds in the cohesively weaker of the two metals.

In Fig. 29(a) a LEED pattern is presented for the (100) surface of copper prior to being contacted by gold. Fig. 29(b) and (c) indicate that same surface after having been contacted by gold. In Fig. 29(b) the diffraction spots have become elongated and by varying electron beam voltage a double set of diffraction spots appear (Fig. 29(c)). AES analysis of the surface indicates transferred gold to the copper. Heating of the surface causes atomic surface rearrangement of the gold and copper as indicated in Fig. 29(d) giving evidence to the possible formation of surface ordering.

Interfacial transfer is also seen with the sliding of one metal across the surface of another with just a single pass. This is indicated in Fig. 30(a) for gold sliding against sputter cleaned rhodium. AES analysis indicates the presence of gold in addition to rhodium peaks.

Even in the presence of metal oxides transfer and wear to one surface will occur with a single pass of a metal across the surface of another metal on an atomistic scale. Fig. 30(b) is an AES spectrum obtained from a palladium crystal surface containing an oxide after a single pass of a gold slider across that surface. The spectrum of Fig. 30(b) indicates the presence of gold on the surface.

The observation that for dissimilar metals in contact the adhesive

interfacial atom bonding is stronger than the cohesive bonding in the cohesively weaker of the two materials is also seen in adhesion experiments in the field ion microscope. An example for such an observation is the solid state interaction of platinum with iridium.

Fig. 31(a) is a field ion micrograph of an iridium surface after cleaning. The (100) atomic plane lies just above the midpoint of the micrograph. After contact with platinum the image of Fig. 31(b) was obtained. Platinum has transferred to the iridium surface in a nearly epitaxial manner. A large dark area appears just below the (100) region of the surface. This is attributed to a contaminant present on the platinum surface.

Field evaporation of the platinum from the iridium surface resulted in the return of the original iridium image as seen in Fig. 31(a). The field evaporation required the removal of two atomic layers from the (100) region to completely remove all platinum and regain the original iridium surface.

The micrographs of Fig. 31 were obtained with simple static contact of the platinum with iridium. Under such conditions the transfer of platinum to iridium occurs in a rather uniform near epitaxial manner. Tangential motion was minimized in such contacts.

Adhesion contacts were also made without normal vibration isolation to determine the effect of slight tangential motions on interfacial transfer with the platinum-iridium couple. The field ion micrograph obtained after such a contact is presented in Fig. 32.

The platinum again transferred to the iridium as it had done in the

experiments of Fig. 31(b). The vibration, however, caused the transfer of large "globs" of platinum as opposed to a uniform thin epitaxial film. The "globs" appear on the bright areas of Fig. 32. Thus, the imposition of a slight tangential motion upon the adhesive junction caused the interfacial transfer (wear) to change in mode from uniform near surface fracture of platinum cohesive bonds to fracture subsurface in the platinum with globular transfer to the iridium.

SUMMARY REMARKS

The atomic nature of solid surfaces plays an important role in the wear behavior for materials in solid state contact. There are a number of tools which can be extremely useful in the study of wear. They include such unsophisticated techniques as simple chemical etching to the use of the field ion microscope with atom probe. These surface devices provide useful information as simple analytical tools to examine wear surfaces as well as to conduct in situ dynamic monitoring of wear studies.

Some devices which have been successfully used by investigators in the study of wear include etch pitting, x-ray diffraction, electron diffraction, scanning electron microscopy, low energy electron diffraction, Auger emission spectroscopy, electron spectroscopy for chemical analysis, field ion microscopy, and the atom probe. Still other devices are available for use.

Analysis of wear surfaces and the wear process with these tools has indicated the anisotropic nature of the wear process. They reveal the role of wear surface and subsurface dislocations in the generation of wear particles and the effect of crystal structure. With dissimilar metals in

contact indication is given by these devices that the cohesively weaker metal transfers to the cohesively stronger with the mode of fracture depending on the type of interfacial motion. A wear mode initiated by cleavage along slip bands in metals has also been identified.

REFERENCES

1. Holm, R., Electrical Contacts, Stockholm, Gerbers, 1946.
2. Burwell, J. T., and Strang, C. P., "Metallic Wear," Proceedings of the Royal Society (London), Vol. 212A, 1952, pp. 470-477.
3. Archard, J. F., "Contact and Rubbing of Flat Surfaces," Journal of Applied Physics, Vol. 24, 1953, pp. 981-988.
4. Krushchov, M. M. and Babichev, M. A., "A Technique for the Selection of Metals for Wear During Sliding on an Abrasive Surface," Izd. Akad. Nauk, SSSR, p. 69, 1941.
5. Rabinowicz, E., Friction and Wear of Materials, Wiley and Sons, Inc., New York, 1965.
6. Suh, N. P., "The Delamination Theory of Wear," Wear, Vol. 25, 1973, pp. 111-124.
7. Vijh, A. K., "The Influence of Solid State Cohesion of Metals and Non-Metals on the Magnitude of Their Abrasive Wear Resistance," Wear, Vol. 35, 1975, pp. 205-209.
8. Rowe, G. W., "Friction, Wear and Lubrication, Terms and Definition," Organization for Economic Co-operation and Development, 1966.
9. Nicholas, J. F., An Atlas of Models for Crystal Surfaces, Gordon & Breach, New York, 1965.
10. Barrett, C. S., Structure of Metal, Crystallographic Methods, Principles, and Data, McGraw-Hill, New York, 1943.

11. McLean, D., Grain Boundaries in Metals, Clarendon Press, Oxford, 1957, p. 16.
12. Bowden, F. P. and Tabor, D., Friction and Lubrication of Solids, Clarendon Press, Oxford, 1954, p. 209.
13. Muller, E. W., and Tsong, T. T., Field Ion Microscopy, Elsevier, New York, 1969, p. 1.
14. Ferrante, J., and Smith, J. R., "A Theory of Adhesion at a Bimetallic Interface: Overlap Effects," Surface Science, Vol. 38, 1973, pp. 77-92.
15. Buckley, D. H., "Adhesion of Metals to a Clean Iron Surface Studied with LEED and Auger Emission Spectroscopy," Wear, Vol. 20, 1972, pp. 89-103.
16. Brainard, W. A., and Buckley, D. H.: "Preliminary Studies by Field Ion Microscopy of Adhesion of Platinum and Gold to Tungsten and Iridium," NASA TN D-6492, 1971.
17. Davisson, C., and Germer, L. H., "Diffraction of Electrons by a Crystal of Nickel," Physical Review, Vol. 30, 1927, pp. 705-740.
18. Farnsworth, H. E., "Penetration of Low Speed Diffracted Electrons," Physical Review, Vol. 49, 1936, pp. 605-609.
19. Estrup, P. J., and McRae, E. G., "Surface Studies by Electron Diffraction," Surface Science, Vol. 25, 1971, pp. 1-52.
20. Lander, J. J., "Auger Peaks in the Energy Spectra of Secondary Electrons From Various Materials," Physical Review, Vol. 91, 1953, pp. 1382-1387.
21. Harris, L. A., "Analysis of Materials by Electron-Excited Auger Electrons," Journal of Applied Physics, Vol. 39, 1968, pp. 1419-1431.
22. Chang, C. C., "Auger Electron Spectroscopy," Surface Science, Vol. 25, 1971, pp. 53-79.

23. Siegbahn, K., et al., ESCA (Electron Spectroscopy for Chemical Analysis) Atomic, Molecular, and Solid-State Structure Studies by Means of Electron Spectroscopy, Nova Acta Regial Soc. Sci. Upsal., 1967.
24. Hercules, S. H., and Hercules, D. M., Characterization of Solid Surfaces, Kane, P. F. and Larrabee, G. B., eds., Plenum Press, New York, 1974, pp. 307-336.
25. Baldwin, B. A., "Chemical Characterization of Wear Surfaces Using X-Ray Photoelectron Spectroscopy," Lubrication Engineering, Vol. 32, 1976, pp. 125-130.
26. Shirley, D. A. (ed.), Electron Spectroscopy, North Holland, Amsterdam, 1972.
27. Johari, O., and Samudra, A. V., Characterization of Solid Surfaces, Kane, P. F. and Larrabee, G. B., eds., Plenum Press, New York, 1974, Ch. 5.
28. Brainard, W. A., and Buckley, D. H., "Dynamic SEM Wear Studied of Tungsten Carbide Cermets," Joint Lubrication Conference, Am. Soc. Lubri. Engrs., Am. Soc. Mech. Engrs., Miami, Florida, Oct. 1975.
29. Kane, P. F., and Larrabee, G. B., Characterization of Solid Surfaces, Plenum Press, New York, 1974.
30. Harkins, W. D., "Energy Relations of the Surface of Solids, I. Surface Energy of the Diamond," Journal of Chemical Physics, Vol. 10, 1942, pp. 268-272.
31. Adamson, A. W., Properties of Surfaces, STP-340, Am. Soc. Testing Mater., Philadelphia, 1963, p. 32.
32. Gilman, J. J., Fracture, B. L. Averbach, et al., eds., Technology Press and J. Wiley, New York, 1959, pp. 193-224.

33. Barrett, C. S., Structure of Metals, Metallurgy and Metallurgical Engineering Series, McGraw-Hill, New York, 1943.
34. Wheeler, D. R. and Buckley, D. H., "Texturing in Metals as a Result of Sliding," NASA TN D-7136, 1973.
35. Shewmon, P. G., "New Method for Measuring Surface Energies and Torques of Solid Surfaces," Transactions of the Metallurgical Society of American Institute of Mining, Metallurgical, and Petroleum Engineers, Vol. 227, 1963, pp. 400-405.
36. Tyson, W. R., "Estimation of Surface Energies from Phonon Frequencies for BCC and FCC Metals," Journal of Applied Physics, Vol. 47, 1976, pp. 459-465.
37. Dyson, B. F., Ph.D Thesis, University of Sheffield, Dept. of Metallurgy, 1962.
38. Buckley, D. H., "Effect of Sulfur, Oxygen, and Hydrogen Sulfide Surface Films on the Adhesion of Clean Iron," International Journal of Non-destructive Testing, Vol. 2, 1970, pp. 171-188.
39. Hondres, E. D., Properties of Surface and Their Measurement, pt. 3, Ch. 8A, National Physical Lab., Leddington, Middlesex, 1972, pp. 293-348.
40. Mykura, H., "The Variation of the Surface Tension of Nickel with Crystallographic Orientation," Acta Metallurgica, Vol. 9, 1961, pp. 570-576.
41. Shewmon, P. G., "New Method for Measuring Surface Energies and Torques of Solid Surfaces," Transactions of the American Institute of Mining, Metallurgical, and Petroleum Engineers, Vol. 227, 1963, pp. 400-405.
42. Blakely, J. M., and Mykura, H., "Surface Self Diffusion and Surface Energy Measurements on Platinum by the Multiple Scratch Method," Acta Metallurgica, Vol. 10, 1962, pp. 565-572.

43. Sundquist, B. E., "A Direct Determination of the Anisotropy of the Surface Free Energy of Solid Gold, Silver, Copper, Nickel, and Alpha and Gamma Iron," Acta Metallurgica, Vol. 12, 1964, pp. 67-86.
44. Nelson, R. S., Mazey, D. J., and Barnes, R. S., "The Thermal Equilibrium Shape and Size of Holes in Solids," Philosophical Magazine, Vol. 11, 1965, pp. 91-111.
45. Barbour, J. P., et al., "Determination of the Surface Tension and Surface Migration Constants for Tungsten," Physical Review, Vol. 117, 1960, pp. 1452-1459.
46. Kumar, R. and Grenga, H. E., "Surface Energy Anisotropy of Iridium," Surface Science, Vol. 50, 1975, pp. 399-406.
47. Jura, G., and Garland, C. W., "The Experimental Determination of the Surface Tension of Magnesium Oxide," Journal of the American Chemical Society, Vol. 74, 1952, pp. 6033-6034.
48. Wawra, H., "Zahlenvergleiche der durch Ultraschalltests oder andere konventionelle Prufmethoden gewonnenen Werte zur Temperaturabhangigkeit der freien Oberflachenergie fester Substanzen," Zeitschrift fur Metallkunde, Vol. 66, 1975, pp. 395-401.
49. Udin, H., Metal Interfaces, Am. Soc. Metals, Metals Park, 1952, p. 114.
50. Obreimoff, J. W., "The Splitting Strength of Mica," Proceedings of the Royal Society (London), Vol. 127A, 1930, pp. 290-297.
51. Gilman, J. J., "Direct Measurements of the Surface Energy of Crystals," Journal of Applied Physics, Vol. 31, 1960, pp. 2208-2218.
52. Buckley, D. H., "Effect of Surface Films on Deformation of Zinc Single-Crystal Surface During Sliding," American Society of Lubrication Engineers Transactions, Vol. 15, 1972, pp. 96-102.

53. Gwathmey, A. T., Leidheiser, H., Jr., and Smith, G. P., Influence of Crystal Plane and Surrounding Atmosphere on Some Types of Friction and Wear Between Metals," NACA TN 1461, 1948, p. 37.
54. Evans, D. M., Layton, D. N., and Wilman, H., "The Deformation of Copper and Iron Crystals by Unidirectional Abrasion," Proceedings of the Royal Society (London), Vol. 205A, 1951, pp. 17-30.
55. Seal, M. and Menter, J. M., "Crystallographic Slip in Diamond," Philosophical Magazine, Vol. 44, 1953, pp. 1408-1410.
56. Agarwala, R. P. and Wilman, H., "The Surface Deformation Caused on Ion Crystals by Unidirectional Abrasion," Proceedings of the Physical Society, London, Vol. 66B, 1953, pp. 717-720.
57. Agarwala, R. P. and Wilman, H., "The Transformation of α -Iron to γ -Iron During Abrasion," Proceedings of the Royal Society (London), Vol. 223A, 1954, pp. 167-174.
58. Buckley, D. H. and Johnson, R. L., "Marked Influence of Crystal Structure on the Friction and Wear Characteristics of Cobalt and Cobalt-Base Alloys in Vacuum to 10^{-9} Millimeter of Mercury., I: Polycrystalline and Single Crystal Cobalt," NASA TN D-2523, 1964, and II: Cobalt Alloys," NASA TN D-2524, 1964.
59. Bowden, F. P., Brookes, C. A., and Hanwell, A. E., "An Anisotropy of Friction in Crystals," Nature, Vol. 203, 1964, pp. 27-30.
60. Steijn, R. P., "On the Wear of Sapphire," Journal of Applied Physics, Vol. 32, 1958, pp. 1951-1958.
61. Riesz, C. H., "Mechanism of Wear of Nonmetallic Materials," WADC-TR-59-316, pt. 2, Armour Research Foundation, 1960.

62. Duwell, E. J., "Wear Rates of Rutile and Spinel Single Crystals in Water-Lubricated Slide Interfaces," American Society of Lubrication Engineers Transactions, Vol. 12, 1969, pp. 34-35.
63. Barquins, M., Kennel, M., and Courtel, R., "Comportement De Monocristaux De Cuivre Sous L'Action De Contact D'Un Frotteur Hemisphenique," Wear, Vol. 11, 1968, pp. 87-110.
64. Barquins, M., and Courtel, R., "Sur la Mise en Evidence des Lignes de Glissements Cristallographiques a l'Interieur d'un Monocristal de Cuivre Sous l'Effet d'une Action de Contact," Comptes Rendus Des Sciences, Vol. 262A, 1966, pp. 707-710.
65. Barquins, M., and Courtel, R., "Sur la Structure et l' Extrusior der Bourrelit Frontal Coral Sur Les Monocristaux par le Frottement (deplacement preliminairi)," Comptes Rendus, Vol. 260, 1965, pp. 1085-1088.
66. Steijn, R. P., "Sliding and Wear in Ionic Crystals," Journal of Applied Physics, Vol. 34, 1963, pp. 419-428.
67. Buckley, D. H., "Friction, Wear, and Lubrication in Vacuum," NASA SP-277, 1971.
68. Gilman, J. J., The Surface Chemistry of Metals and Semiconductors, H. C. Gatos, ed., Wiley, New York, 1960, p. 136.
69. Bailey, J. M., and Gwathmey, A. T., "Plastic Deformation During Friction and Wear on Single Crystals of Copper," Proc. of the American Chemical Society, Petroleum Division Symposium, Chemistry of Friction and Wear, Vol. 3, 1958, pp. A25 to A38.

70. Buckley, D. H., "Influence of Chemisorbed Films of Various Gases on Adhesion and Friction of Tungsten," Journal of Applied Physics, Vol. 39, 1968, pp. 4224-4233.
71. Chapman, J. A., and Menter, J. W., "A Study of the Shape, Surface Structure and Frictional Wear of Fibers by Reflexion Electron Microscopy," Proceedings of the Royal Society (London), Vol. 226, 1954, pp. 400-407.
72. Skinner, J., Gane, N., and Tabor, D., "Micro-friction of Graphite," Nature Physical Science, Vol. 232, 1971, pp. 195-196.
73. Gane, N., and Skinner, J., "The Friction and Scratch Deformation of Metals on a Microscale," Wear, Vol. 24, 1973, pp. 207-217.
74. Brainard, W. A., and Buckley, D. H., "Adhesion, Friction, and Wear of a Copper Bicrystal With (111) and (210) Grains," NASA TN D-7232, 1973.

Table 1 Surface energies for various planes
of crystalline solids

Crystalline solid	Structure	Surface energy [32] (ergs/cm ²)				
		Atomic plane				
		(100)	(110)	(111)	(0001)	(1010)
MgO	Rock salt	1310	2330			
Si	Diamond	1350	1270	887		
W	B.C.C.	4680	3320	8130		
α -Fe	B.C.C.	1440	1710	5340		
Cu	F.C.C.	590	820	2980		
Zn	H.C.P.				185	850
Cd	H.C.P.				226	730
C	Graphite				27	2340

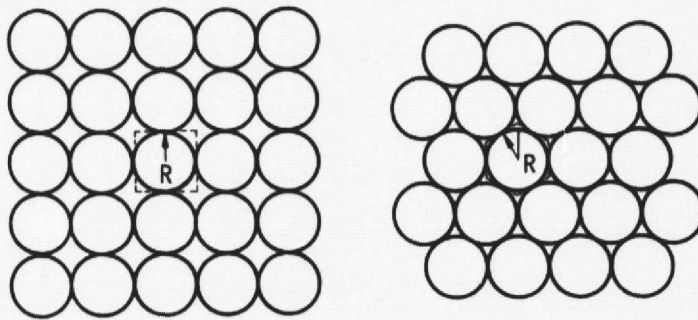


Figure 1. - Arrangement of atoms in surface planes.

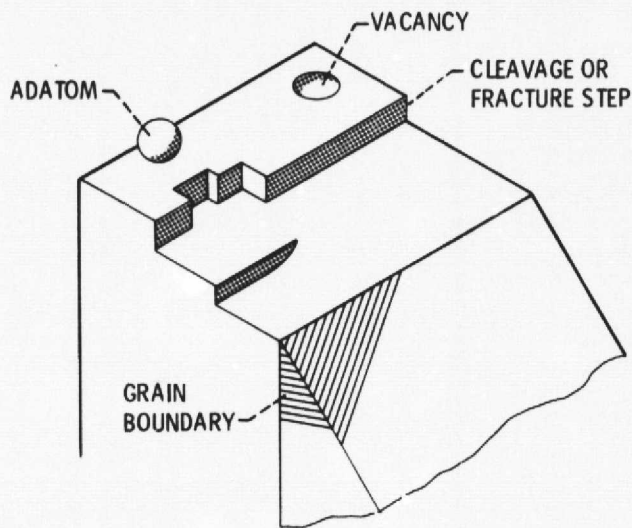


Figure 2. - Model of surface with defects.

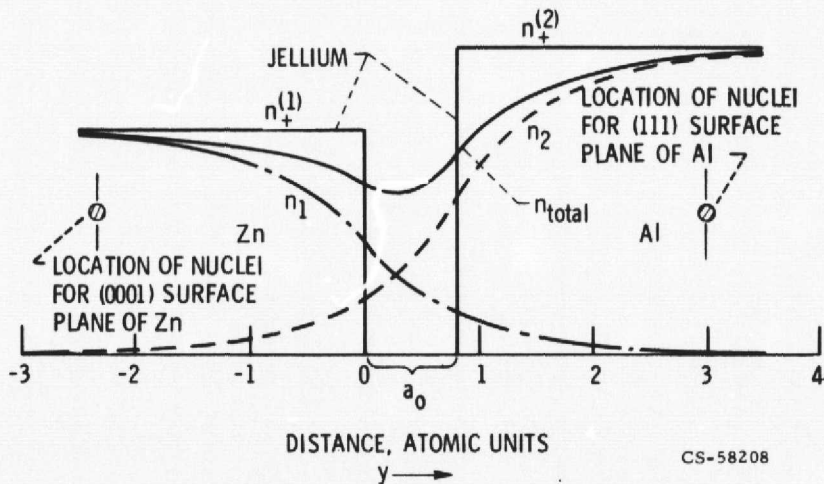


Figure 3. - Jellium charge density to scale for Al-Zn. n_1 and n_2 denote the metal-vacuum electron number densities for Zn and Al respectively

E-0792

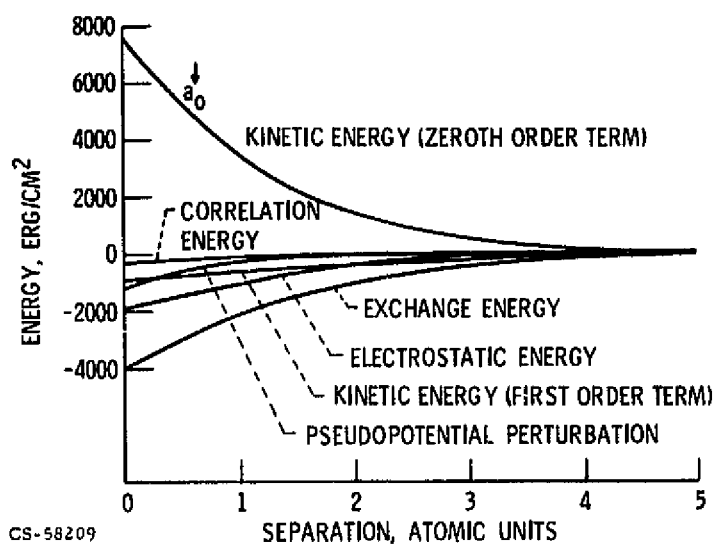


Figure 4. - Energy components for the typical case of Al-Zn. a_0 is the location of the energy minimum

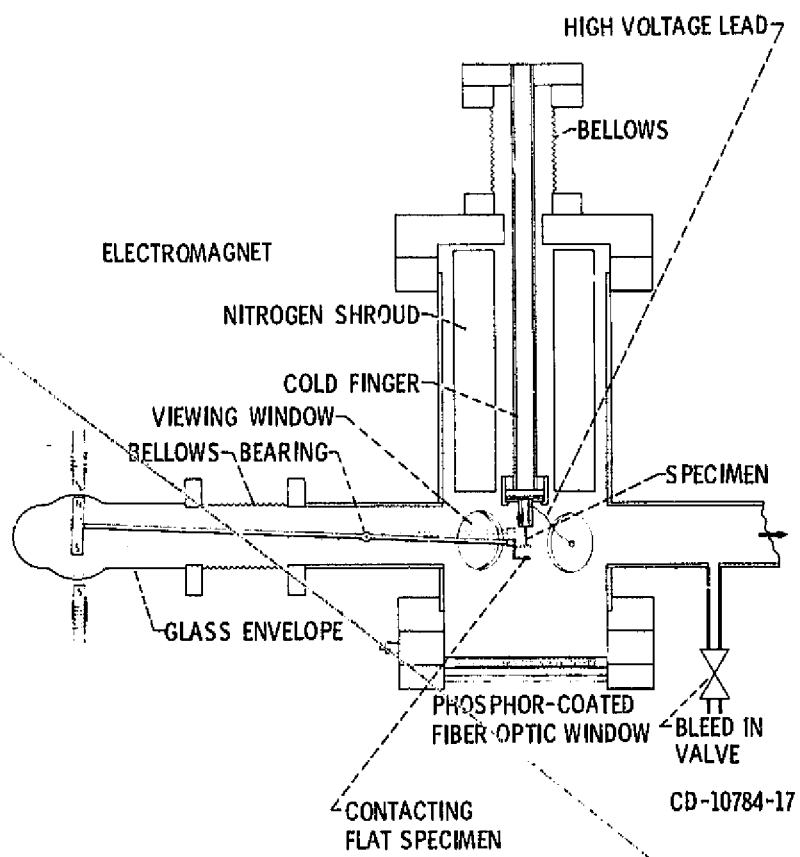


Figure 5. - Diagram of the FIM-adhesion apparatus.

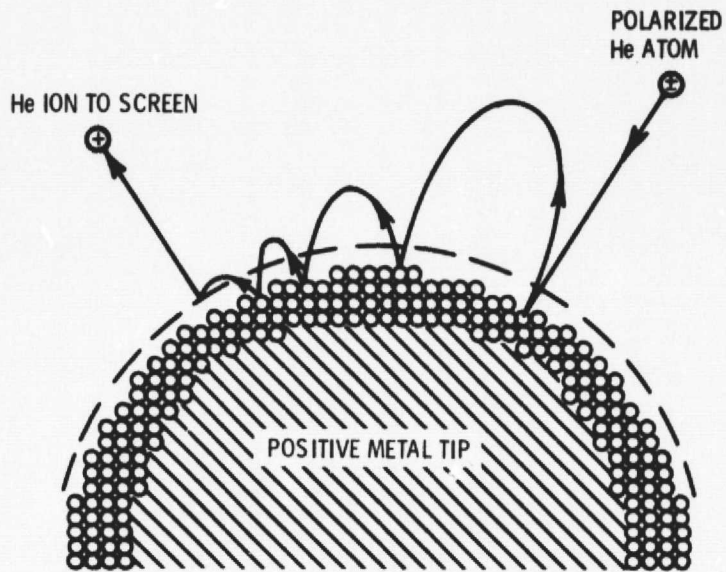


Figure 6. - The principle of field ion microscope image formation.

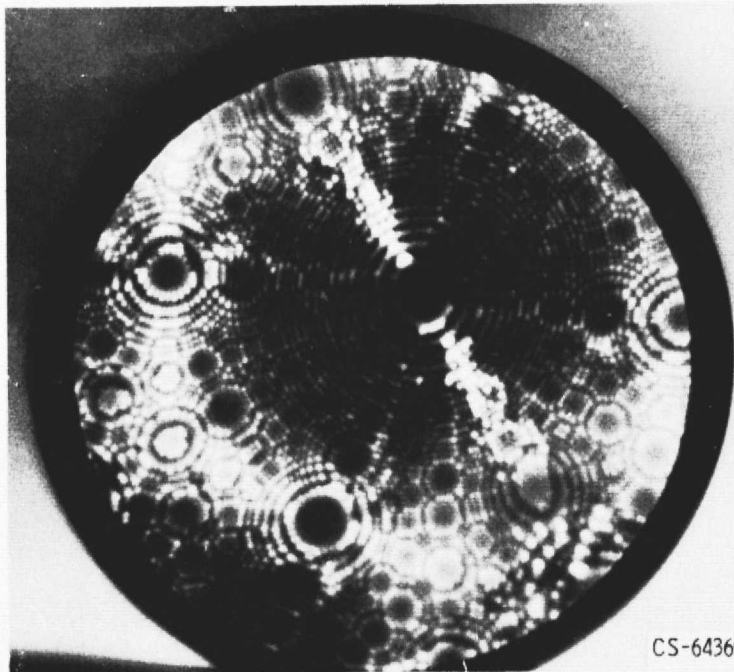


Figure 7. - Field ion microscope pattern on a clean tungsten tip oriented in the (110) direction.

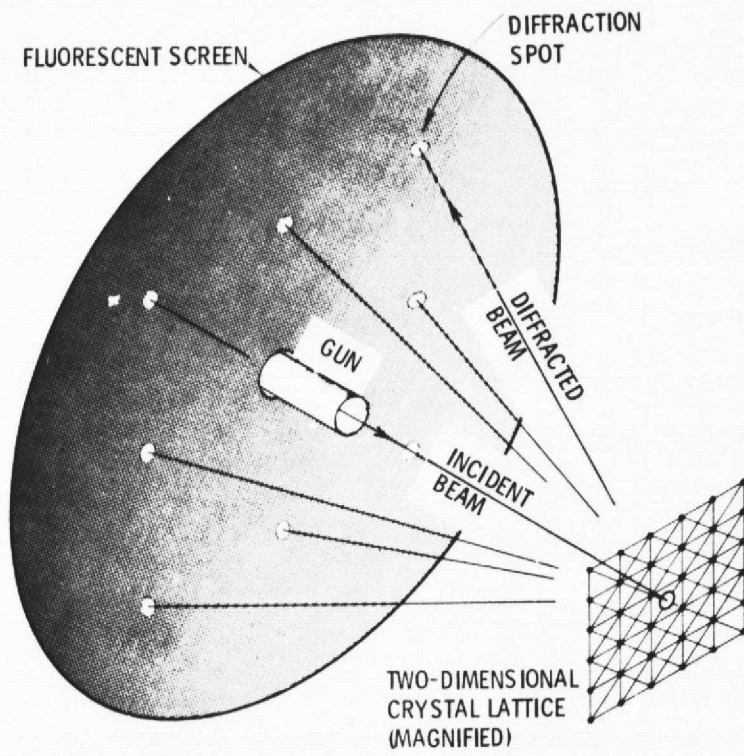
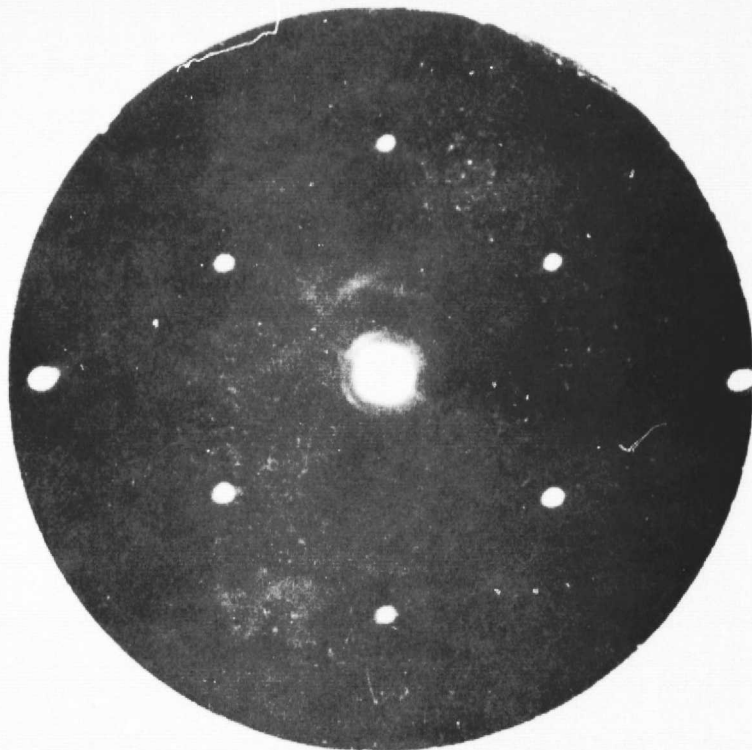
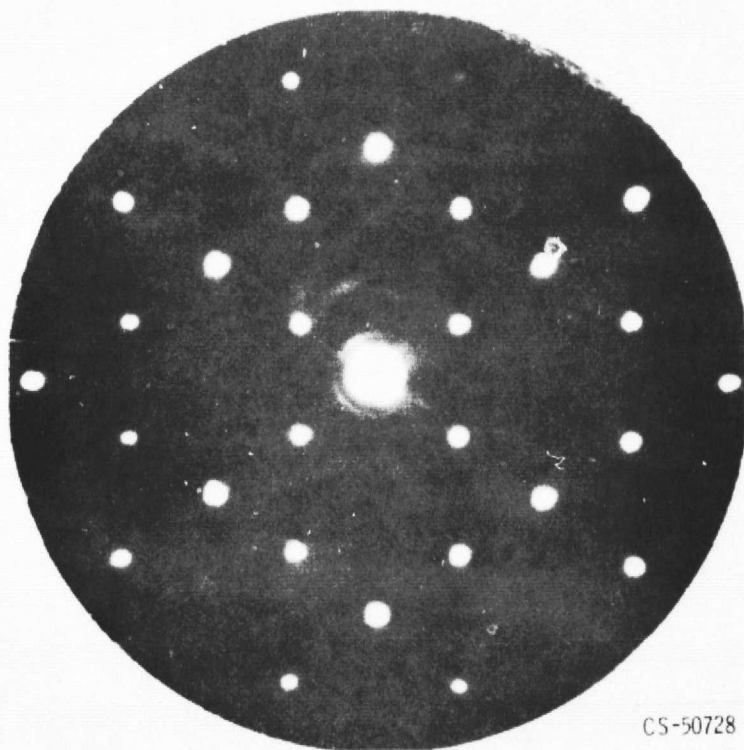


Figure 8. - Formation of diffraction pattern.



CLEAN



CS-50728

1/2 MONOLAYER OF OXYGEN

Figure 9. - LEED pattern for clean and oxidized W (110). $E_0 = 119$ eV.

F-0792

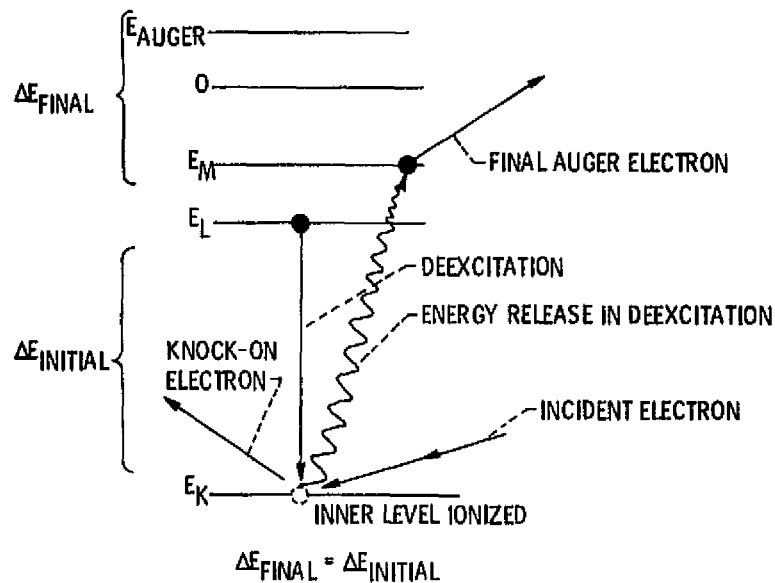


Figure 10. - Auger transition diagram for an atom.

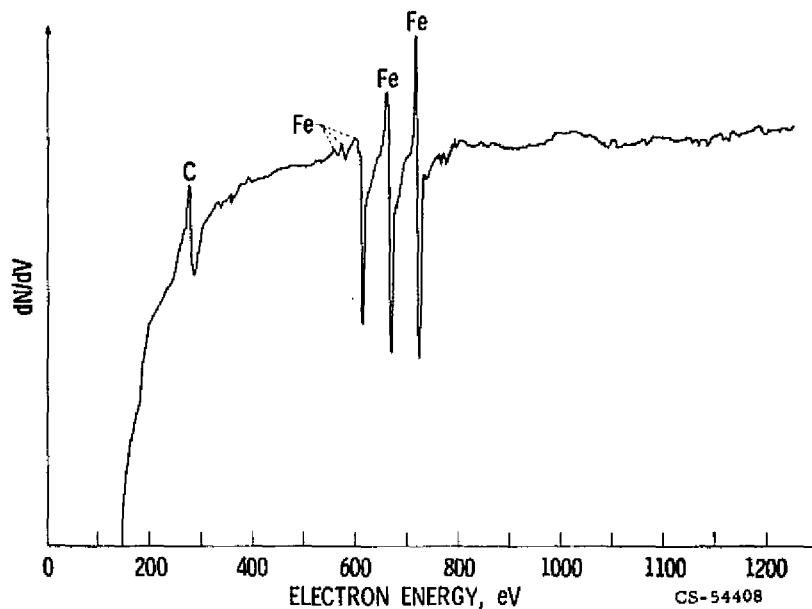


Figure 11. - Derivative of electron energy distribution for ethylene adsorbed on an Fe(001) surface.

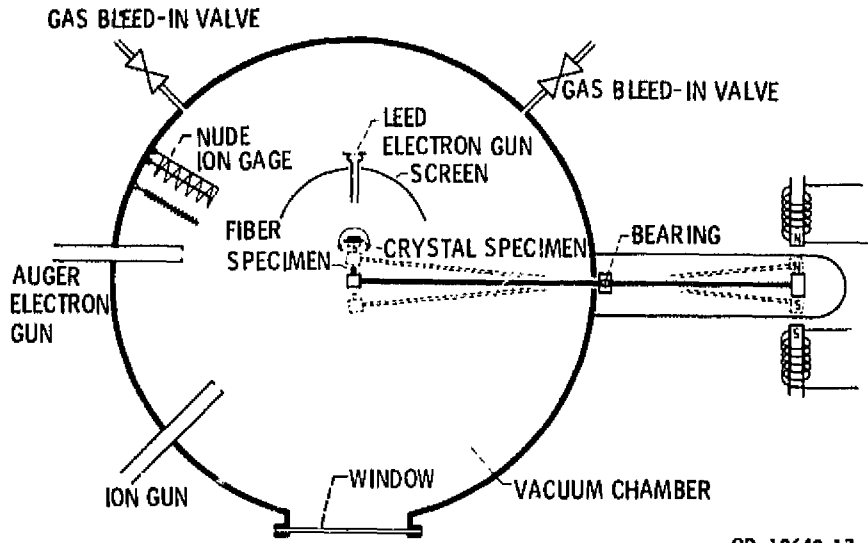


Figure 12. - Low-energy electron-diffraction (LEED) adhesion apparatus.

CD-10640-17

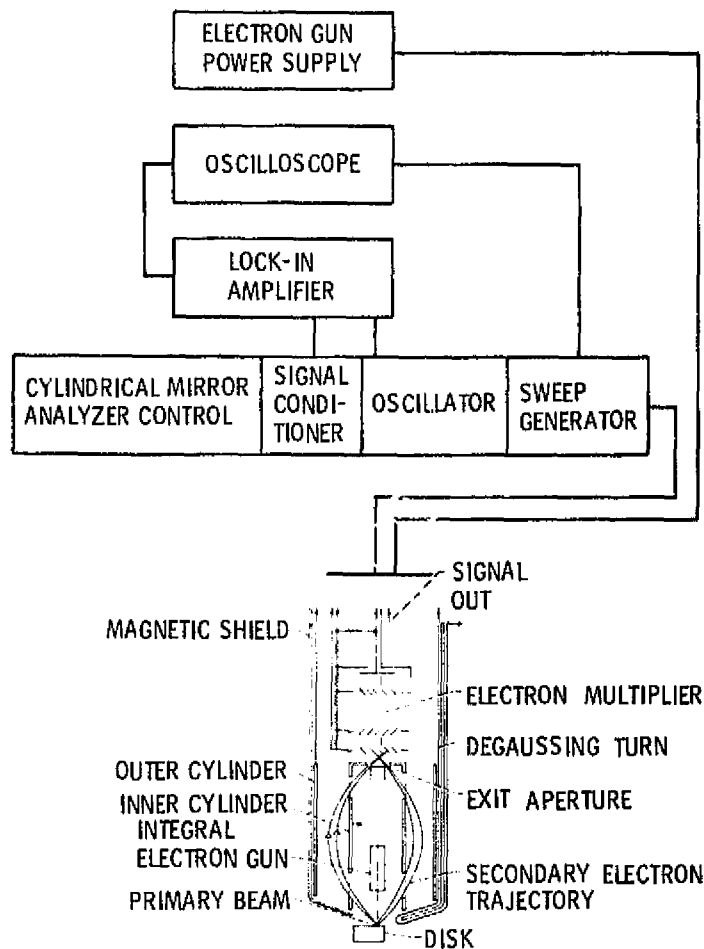


Figure 13. - Block diagram of Auger cylindrical mirror analyzer.

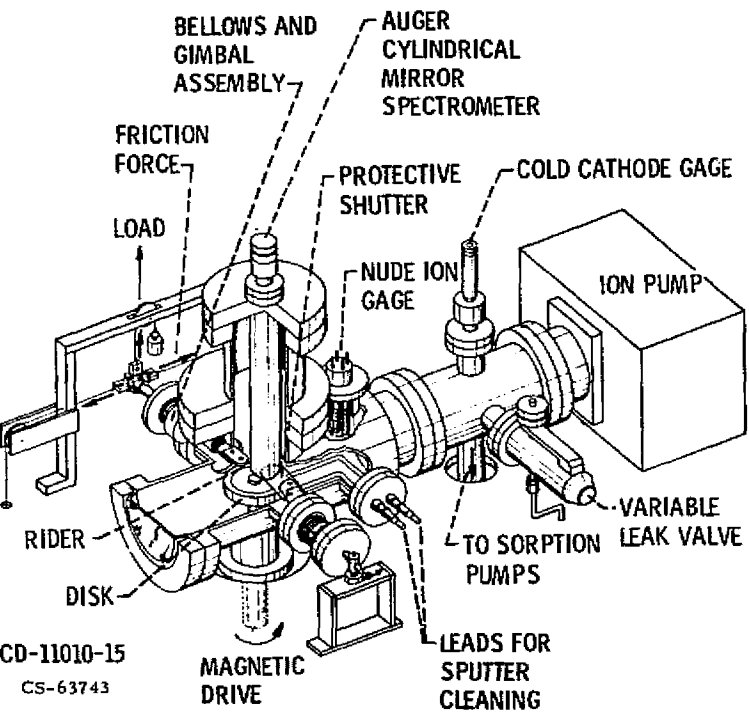


Figure 14. - Friction and wear pin and disk apparatus equipped with Auger electron spectrometer.

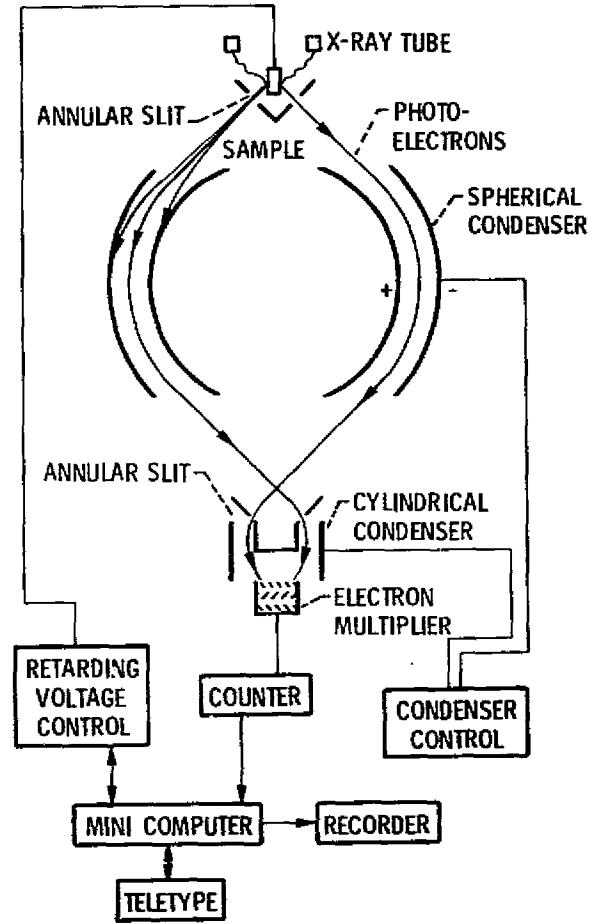


Figure 15. - Schematic of x-ray photoelectron spectrometer (ref. 25).

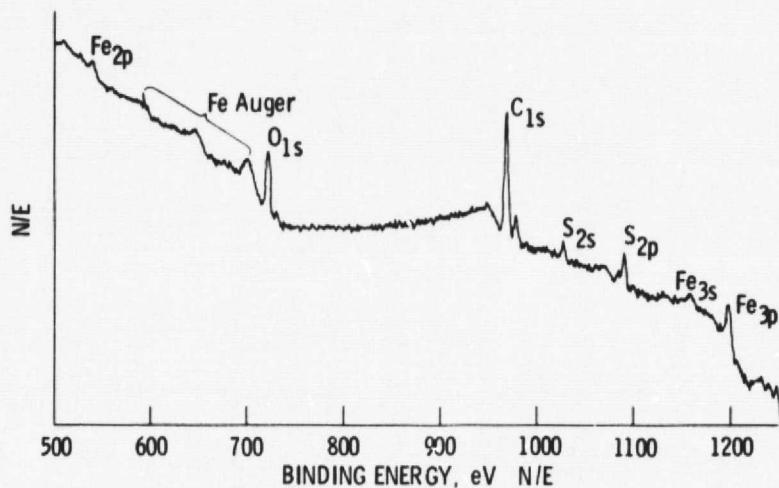


Figure 16. - ESCA spectrum for iron immersed in one percent Dibenzyl Disulfide in mineral oil for one minute at 250°C.

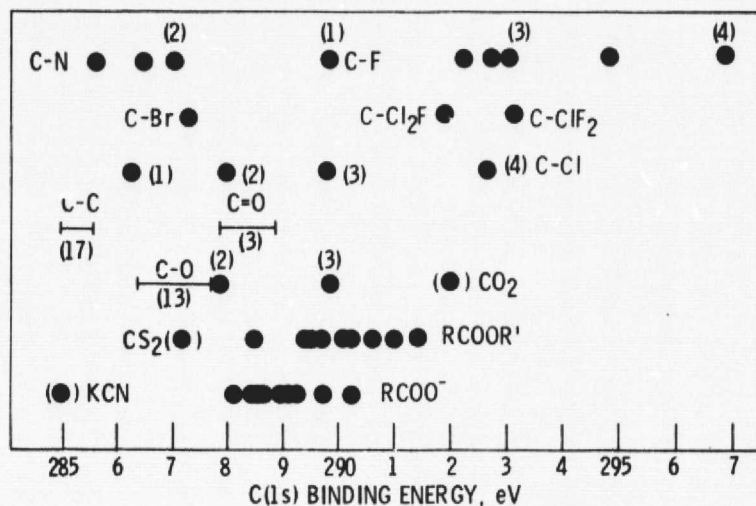


Figure 17. - Correlation chart for carbon 1s electron binding energies and functional groups. (24) — = Range of observed energies for a given bond, (n) = number of compounds used for the range above. (●) = energies observed for single compounds. () = number of atoms attached to carbon, and ● = individual binding energies. The particular functional group compound or bond is shown beside the range or individual points.

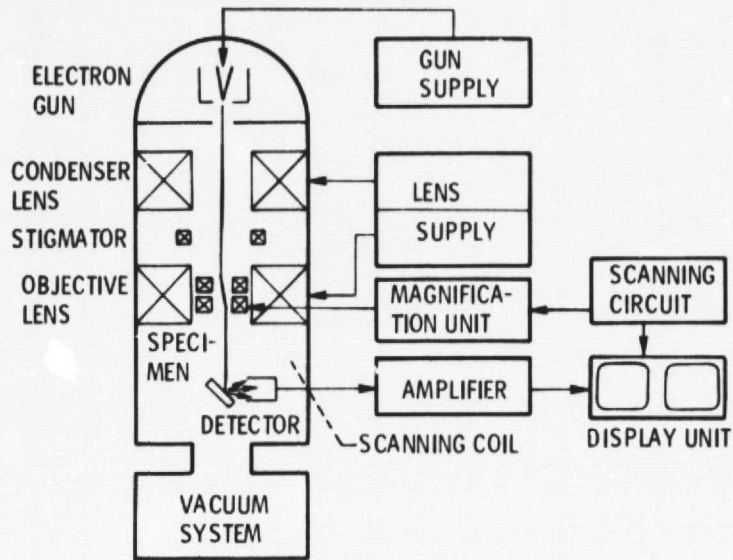


Figure 18. - Simplified block diagram of scanning electron microscope (ref. 27).

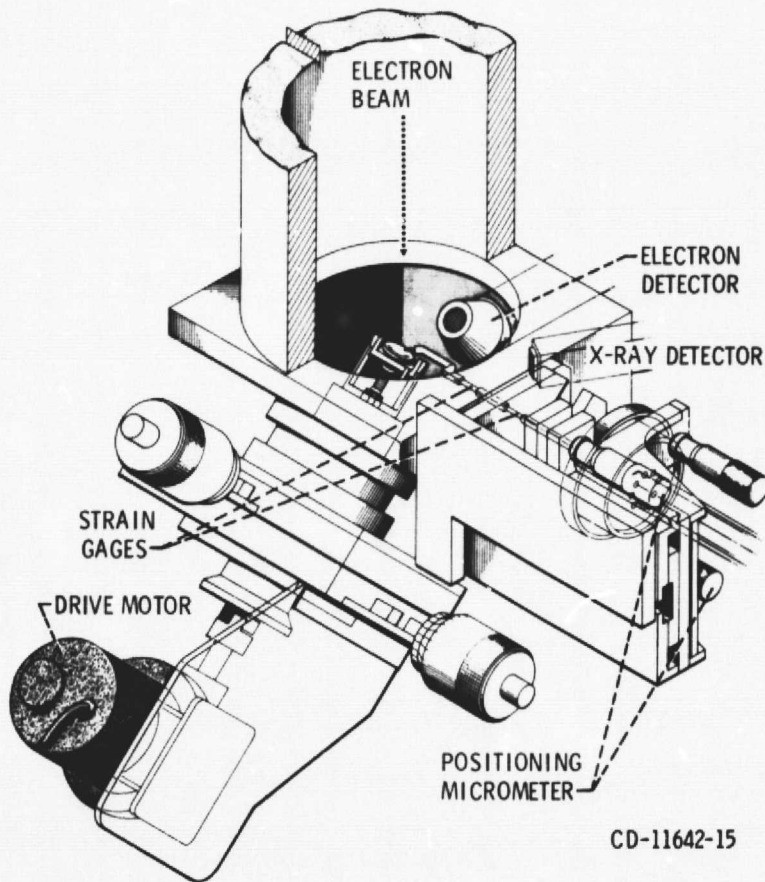


Figure 19. - Detailed drawing of wear apparatus mounted on scanning electron microscope.

CD-11642-15

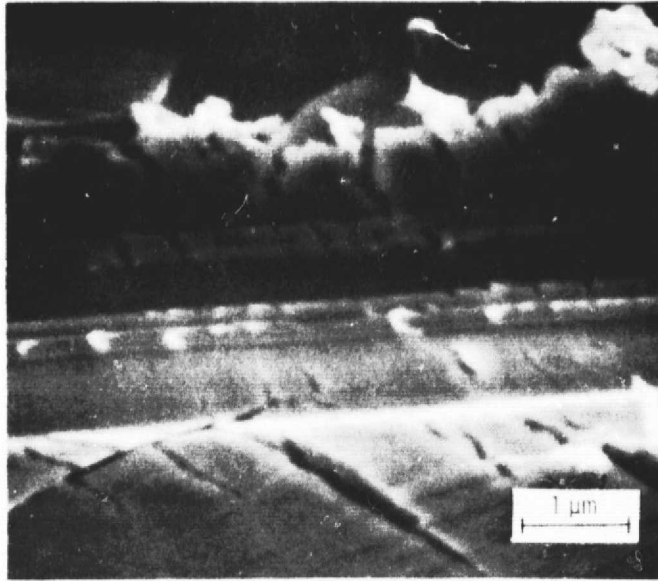
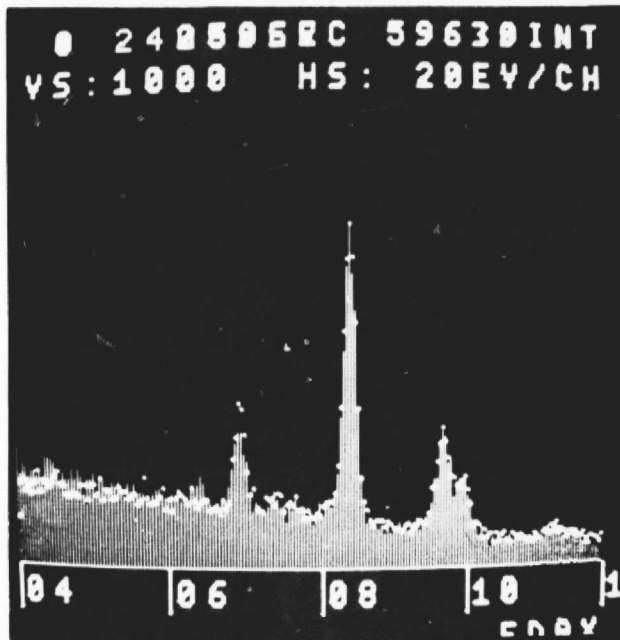
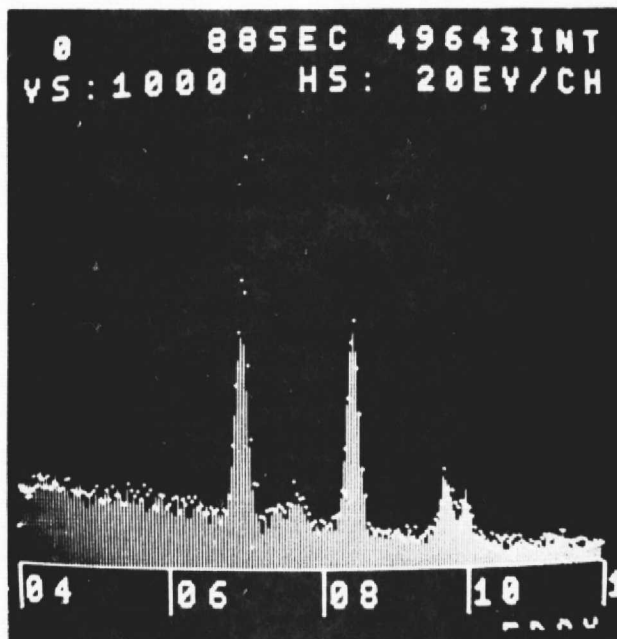


Figure 20. - Single pass of 50 μm diamond stylus on WC.

ORIGINAL PAGE IS
OF POOR QUALITY



6 PERCENT Co-WC



15 PERCENT Co-WC

Figure 21. - Energy dispersive x-ray profiles of wear debris from unetched surfaces compared to bulk surface profiles.

ORIGINAL PAGE IS
 OF POOR QUALITY

- | | |
|---|--|
| AES - Auger electron spectroscopy | ISS - ion scattering spectroscopy |
| EM - electron microscopy | PES - photoelectron spectroscopy |
| EMP - electron microprobe | RUTHERFORD - Rutherford scattering |
| ESCA - electron spectroscopy for chemical analysis | SCANIR - surface composition by analysis of neutral and ion impact radiation |
| IEX - ion excited X-ray fluorescence and ion impact radiation | SEM - secondary electron microscopy |
| IMMA - ion microprobe mass analyzer | SIMS - secondary ion mass spectroscopy |
| | XRF - X-ray fluorescence |

EXCITATION	TECHNIQUES	DETECTION
$h\nu$	XRF ESCA PES AES	$h\nu$
e^-	EMP SEM AES EM IEX SCANIR SEM	e^-
IONS	IMMA SIMS ISS RUTHERFORD	IONS

Figure 22. - Excitation and detection systems used in surface analysis.

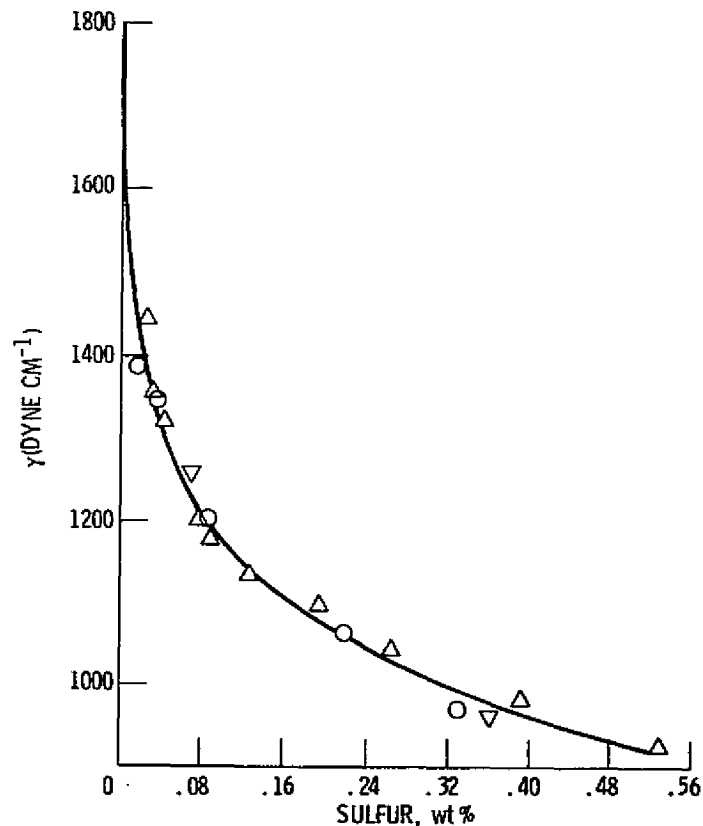


Figure 23. - Dependence of surface energy of liquid iron on sulfur content (ref. 36).

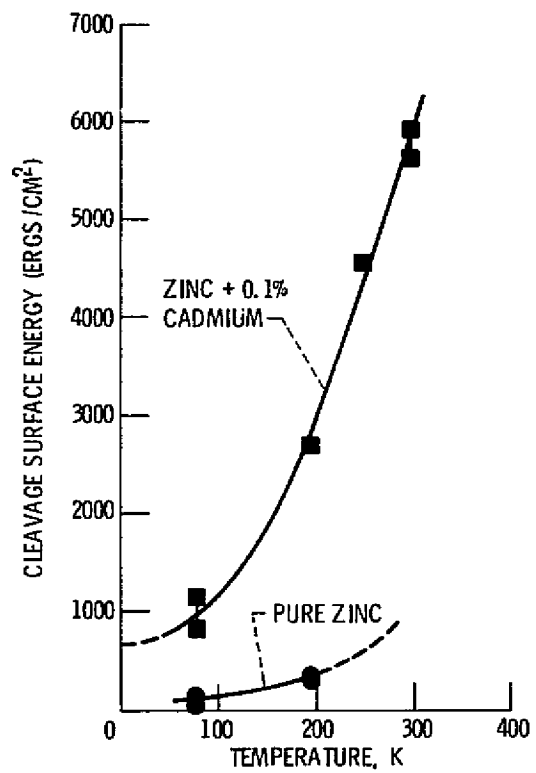


Figure 24. - Effect of temperature on the cleavage of zinc (ref. 51).

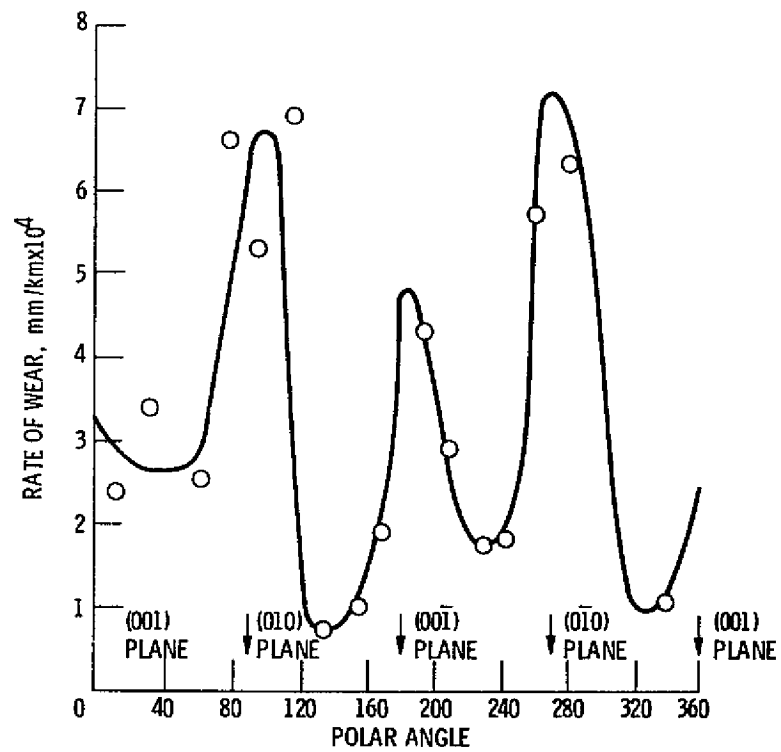


Figure 25. - Rate of wear of a rutile single-crystal sphere on a great circle in the plane of the a- and c-axes. The c-axis is normal to plane of sliding at 0 and 180°. Slide direction in plane of the great circle (ref. 62).

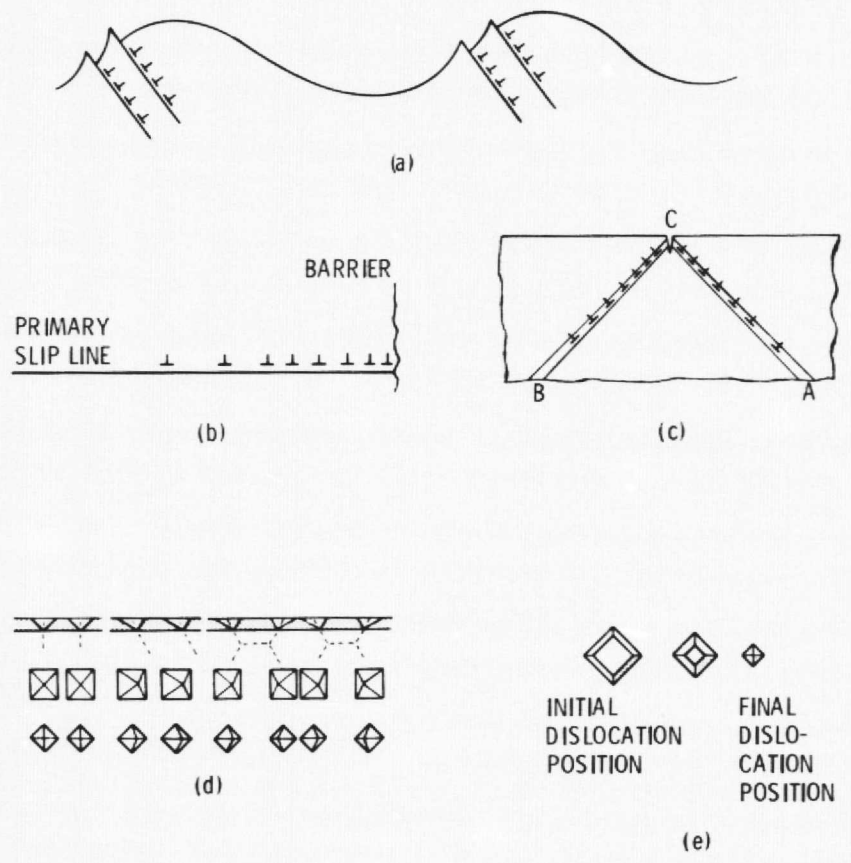
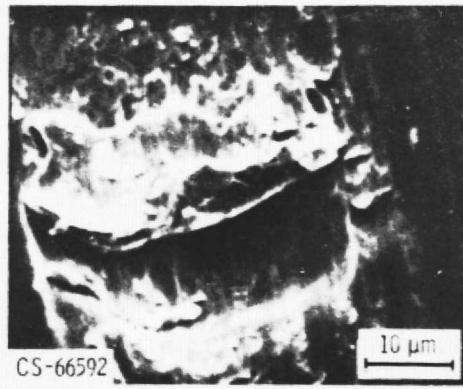


Figure 26. - Dislocations and etch pitting.



(111) GRAIN



(210) GRAIN

Figure 27. - Wear tracks on bicrystal grains. Copper slider; load, 100 g; sliding speed, 1.4 mm/min.

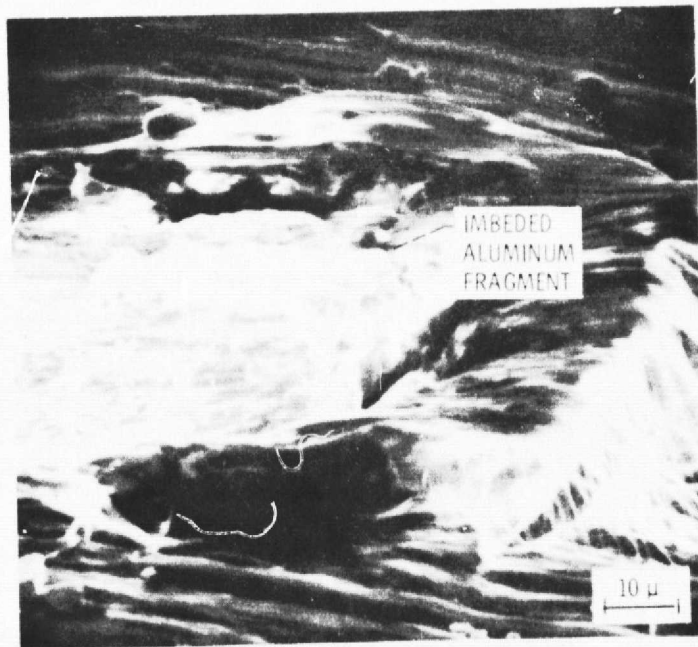
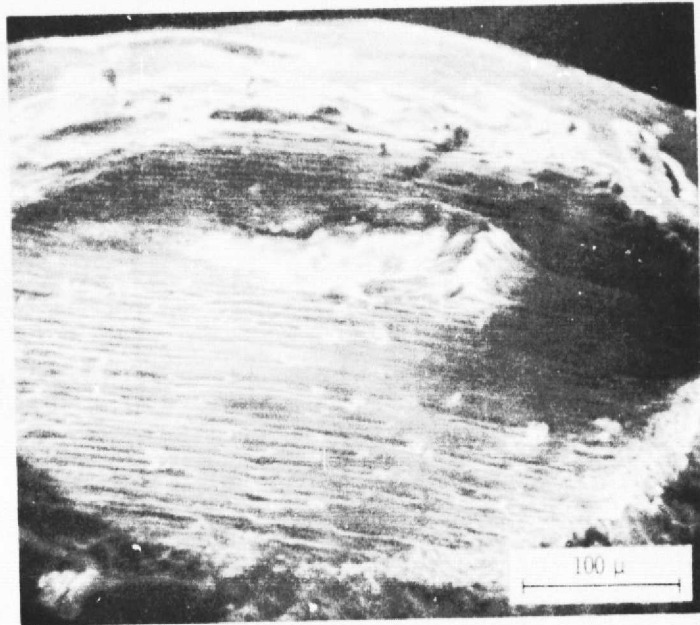
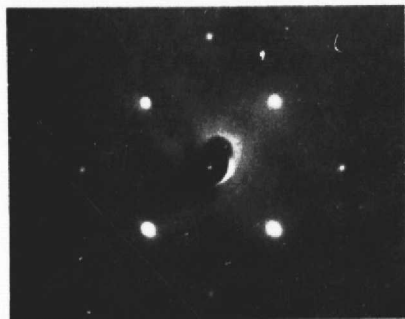
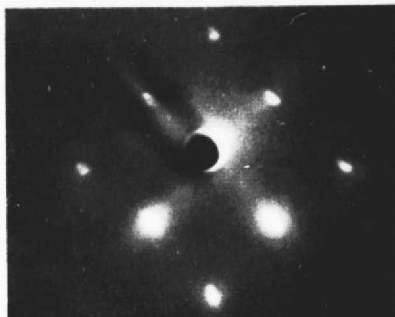


Figure 28. - PTFE - rider-wear scar showing lodged metal fragment run on (110) aluminum surface, single pass, 200 grams.

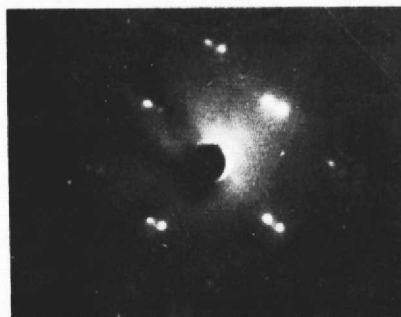
ORIGINAL PAGE IS
OF POOR QUALITY



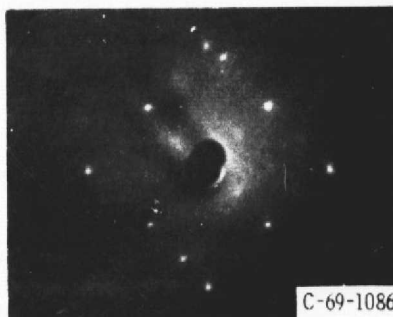
(a) CLEAN COPPER (100) AT 110 VOLTS.



(b) AFTER CONTACT WITH GOLD (100)
UNDER 20-MILLIGRAM LOAD AT 75
VOLTS.



(c) SAME AS (b) BUT AT 140 VOLTS.

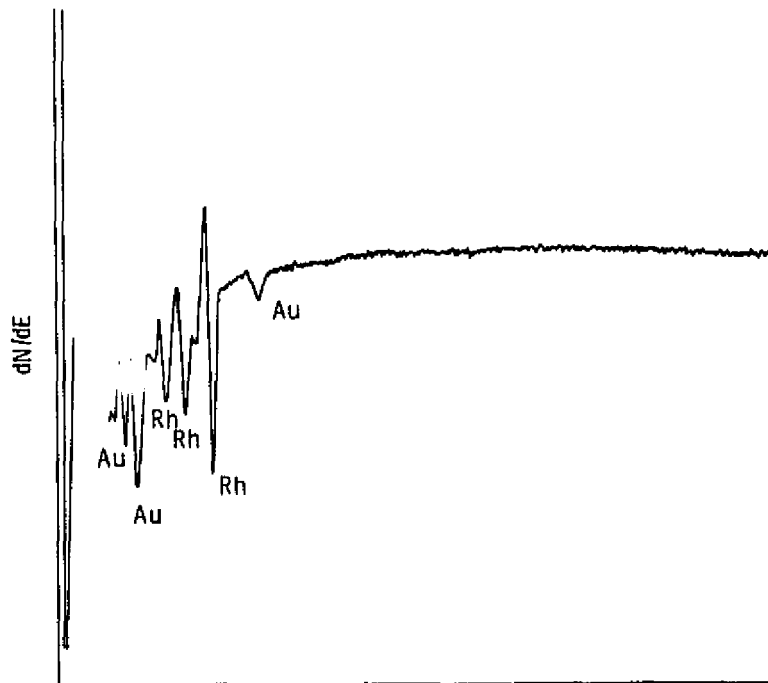


(d) SAME AS (b) AND (c) AFTER HEATING
TO 200⁰ C FOR 30 MINUTES.

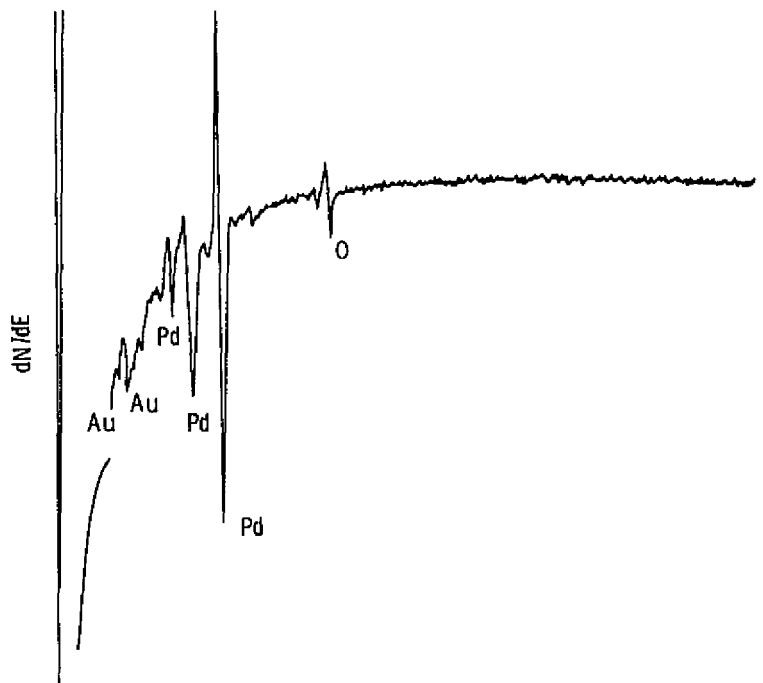
Figure 29. - LEED photographs of copper (100) surface before and after adhesive contact with gold (100) surface.

1-6792

ORIGINAL PAGE IS
OF POOR QUALITY



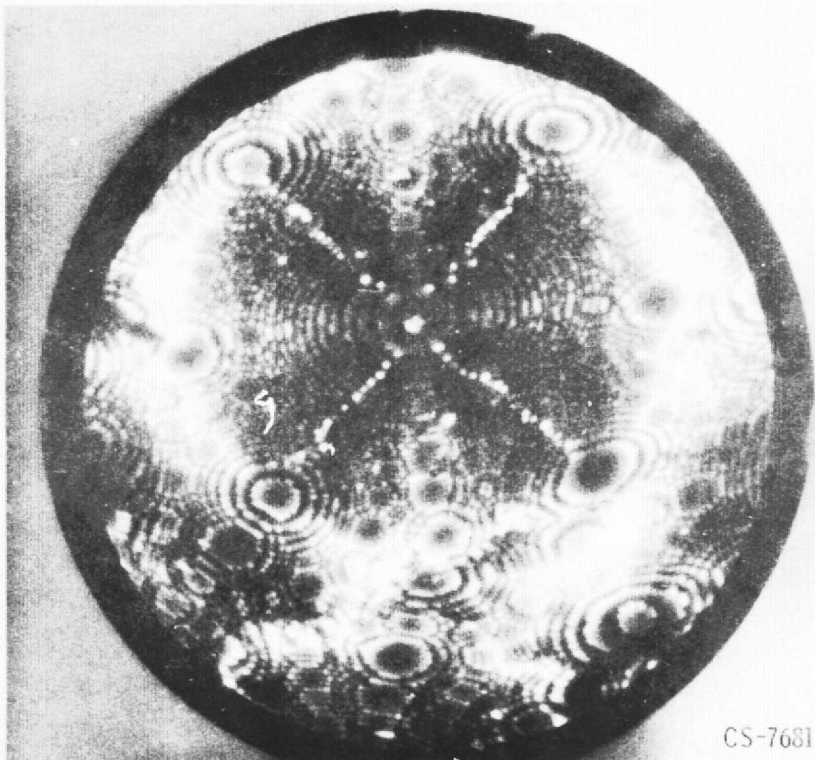
(a) RHODIUM (111).



(b) PALLADIUM (111).

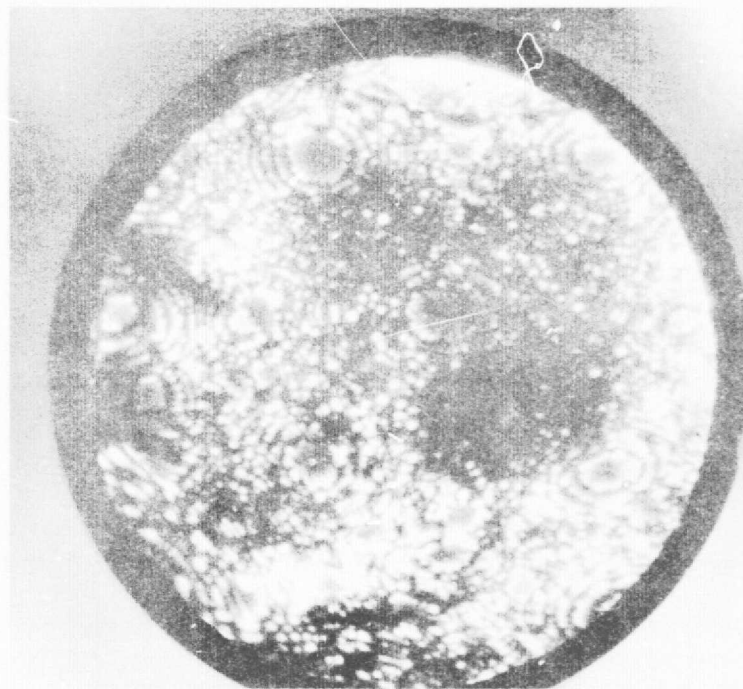
Figure 30. - Auger emission spectrum for a rhodium (111) and a palladium (111) surface containing oxide after a single pass sliding of a gold (111) crystal across the surface. Sliding velocity 0.7 mm/min, load 10 grams, 10^{-10} torr and 23° C.

ORIGINAL PAGE IS
OF POOR QUALITY



CS-76816

(a) Iridium prior to contact.



(b) IRIDIUM AFTER PLATINUM CONTACT AT 19.0 KILOVOLTS.

Figure 31. - Continued.

Figure 31. - Field ion micrographs of iridium-platinum contact. Image gas, helium; liquid-nitrogen cooling.

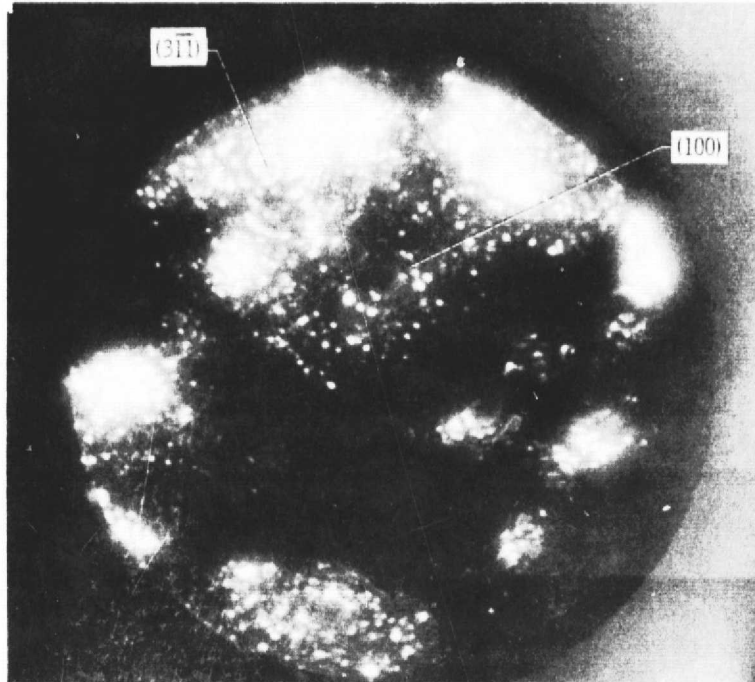


Figure 32. - Iridium after platinum contact at 28.0 kilovolts. No vibration isolation; image gas, helium; liquid-nitrogen cooling. CS-76915

ORIGINAL PAGE IS
OF POOR QUALITY